Subcellular Localization of Apoptosis Initiator NGFI-B is Regulated by MAP Kinase ERK and Apoptosis Signals

Trude Movig

Master's thesis

Department of Biology

UNIVERSITY OF OSLO

June 2007

Acknowledgements

The work presented in this thesis was carried out at the Department of Pharmaceutical Biosciences, University of Oslo, from August 2005 to June 2007 for the Master's degree in Toxicology.

My gratitude goes to my supervisor, Professor Ragnhild Paulsen, for being a great source of inspiration and knowledge and for her mentoring. I would also like to thank my co-supervisor, Karen Debernard, for her invaluable help, experience, and patience.

Beside my supervisors, I also thank Mona Gaarder, Gro Mathisen, Petra Aden, and Bjorn-Oddavar Strom of the Paulsen group for technical assistance and helpful discussions.

My thanks go to everyone at the Department of Pharmaceutical Biosciences for a welcoming environment, and appreciation is given to Berit Syvertsen and Professor Tor Gjoen for assistance with the microscopes.

Thanks also to Tuva Baroy, Marius Gudbrandsen, Ingrid Andersen, Elizabeth Aitken, and Bjorn-Oddvar Strom, and for proof-reading this thesis.

I am very grateful to my boyfriend, my family, and my friends for their support and encouragement.

Oslo, June 2007
Trude Movig

Abstract

NGFI-B (nerve growth factor-inducible clone B) is a nuclear receptor that has been implicated in both cell survival and cell death. In the nucleus, NGFI-B exerts its functions as a transcription factor that promotes survival and proliferation, while translocation of NGFI-B to the mitochondria promotes apoptosis. This unique property of NGFI-B makes it a possible therapeutic target. Many questions concerning the translocation of NGFI-B remain to be solved.

This thesis will investigate several issues regarding the regulation of NGFI-B migration. Nuclear fluorescence recovery after photobleaching (FRAP)-studies in CV-1 cells suggested that the nuclear import of GFP-tagged NGFI-B was energy dependent, and therefore could be regulated by nuclear import mechanisms.

The threonine 142 residue of NGFI-B was previously demonstrated to be phosphorylated by the MAP kinase ERK2, which is activated by growth factor EGF. Whether the nuclear import of NGFI-B was regulated by phosphorylation of threonine 142 of NGFI-B was investigated by FRAP studies of two NGFI-B mutants. A 142 threonine to alanine mutation in NGFI-B that blocked phosphorylation of this residue did not affect the nuclear import of NGFI-B, while a threonine to glutamate mutation that mimicked constitutive phosphorylation possibly decreased the nuclear import of NGFI-B. Additional FRAP studies showed that EGF and ERK2 reduced the nuclear import of NGFI-B.

Cultured cerebellar granule neurons (CGN) which are extensively used in studies of glutamate-induced toxicity, important in stroke and neurodegenerative diseases, were used as an *in vitro* model for studies of neuronal apoptosis. Cell death of CGN induced by glutamate appeared to be slightly reduced by inhibition of the MEK/ERK pathway, contrarily to EGF-induced ERK activation which is reported to be involved in neuronal survival. The translocation of NGFI-B out of the nucleus demonstrated by immunostaining after glutamate exposure suggests that CGN may be used as a model for determination of neuronal NGFI-B traffic.

In conclusion, the subcellular localization of apoptosis initiator NGFI-B is regulated by MAP kinase ERK and apoptosis signals.

Contents

Abbreviations

Ad	Up to
ADC	Analog-to-digital converter
AF	Activation function
AIF	Apoptosis-inducing factor
AMPA	α-amino-3-hydroxy-5-methyl-4-isoxazolepropionic acid
ANOVA	Analysis of variance
Apaf-1	Apoptotic protease-activating factor 1
Ara-C	Cytosine β-D-arabino-furanoside
BBS	BES buffered saline solution
Bcl-2	B-cell lymphoma protein 2
BES	N,N-Bis-(2-hydroxyethyl)-2-aminoethanesulfonic acid
BH	Bcl-2 homology
BME	Basal medium eagle
BSA	Bovine serum albumin
CGN	Cerebellar granule neurons
CLSM	Confocal laser scanning microscope
DAPI	4',6-diamidino-2-phenylindole
DBD	DNA-binding domain
DIC	Differential interference contrast
DMEM	Dulbecco's modified Eagle's medium
DMSO	Dimethyl sulfoxide
DnaseI	Deoxyribonuclease I
DTT	Dithiothreitol
EDTA	Ethylenediaminetetraacetic acid
EGF	Epidermal growth factor
ERK	Extracellular signal-regulated kinase
FBS	Fetal bovine serum
FITC	Fluorescein isothiocyanat
FRAP	Fluorescence recovery after photobleaching
GFP	Green fluorescent protein
HEPES	4-(2-hydroxyethyl)-1-piperazineethanesulfonic acid

JNK	Jun N-terminal kinase
LBD	Ligand binding domain
MAP	Mitogen activated protein
MAPK	Mitogen-activated protein kinase
MEK	MAPK/ERK kinase
MES	2-(*N*-morpholino)ethanesulfonic acid
MQ	Milli Q
NBRE	NGFI-B Response Element
NES	Nuclear export signal
NGF	Nerve growth factor
NGFI-B	Nerve growth factor inducible clone B
NLS	Nuclear localization signal
NMDAR	*N*-methyl-d-aspartate receptor
NPC	Nuclear pore complex
Nups	Nucleoporins
NurRE	Nur-responsive element
PBS	Phosphate buffered saline
PFA	Paraformaldehyde
RLU	Relative luciferase units
ROS	Reactive oxygen species
SD	Standard deviation
SE	Standard error
TCA	Trichloroacetic acid
Tris	Trishydroxymethylaminomethane
wt	Wild type

1 Introduction

1.1 Nerve Growth Factor-Inducible Clone B

Nerve growth factor-inducible clone B (NGFI-B) was originally identified in rat as a transcription factor that was rapidly induced by nerve growth factor (NGF) (Milbrandt, 1988). The equivalent protein in mouse is called Nur77 (Hazel *et al.*, 1988), and the human homologue is termed TR3 (Chang *et al.*, 1989). NGFI-B, and the closely related proteins RNR-1 (also known as Nurr 1, TINUR and HZF-3) and Nor-1 (MINOR, CHN and TEC), form a distinct subfamily (NR4A1-3) within the nuclear receptor superfamily as immediate–early genes induced by multiple signal transduction pathways (Clark *et al.*, 1996; de Ortiz *et al.*, 1994; Hedvat and Irving, 1995; Labelle *et al.*, 1995; Law *et al.*, 1992; Martinez-Gonzalez and Badimon, 2005; Ohkura *et al.*, 1994; Okabe *et al.*, 1995; Scearce *et al.*, 1993). This subgroup is classified as orphan receptors since a physiological ligand for the receptors has not yet been identified (Wang *et al.*, 2003).

The nuclear receptor NGFI-B has an estimated molecular mass of approximately 61 kDa (Fahrner *et al.*, 1990), and is composed of four distinct structural domains. The amino-terminal A/B region contains the activation function 1 (AF-1) domain, which is required for the recruitment of transcriptional co-activators (Figure 1.1). The C region consists of a DNA-binding domain (DBD) with two cysteine rich zinc-finger motifs and a downstream A-box. This A box is essential for high affinity binding of NGFI-B to the NGFI-B response element (NBRE), which is within the 5'-region of target genes (Wilson *et al.*, 1992). Monomeric NGFI-B binds to the two 5' adenosine nucleotides in the NBRE consensus sequence 5'AAAGGTCA3' (Wilson *et al.*, 1991). Homodimers bind to an inverted repeat of a NBRE-related octanucleotide, the Nur-responsive element (NurRE) (Philips *et al.*, 1997). The D domain includes a hinge region which participates in the formation of dimers. The E/F region is located to the carboxyl-terminal of the NGFI-B protein, and contains a dispensable transcriptional activation domain, activation function 2 (AF-2), and also an atypical C-terminal ligand binding domain (LBD) without the classical hydrophobic cleft for ligand binding (Mangelsdorf and Evans, 1995; Wansa *et al.*, 2003).

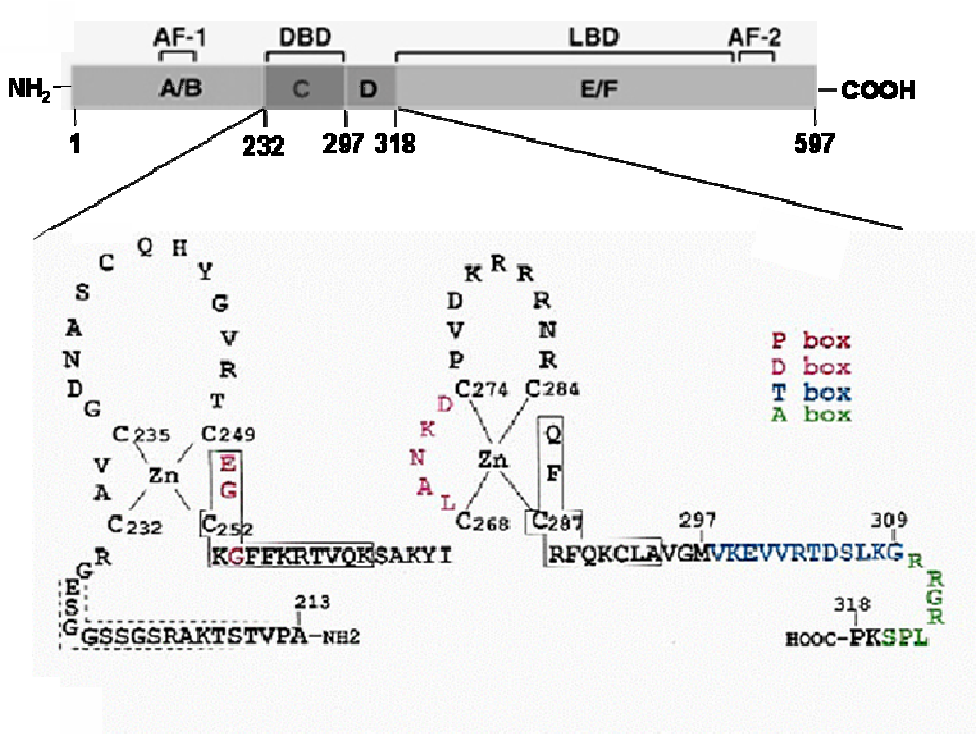

Figure 1.1: Schematic illustration of NGFI-B with regions A through E.
The top panel shows the domain structure of NGFI-B, AF-1, DBD, LBD, and AF-2 (see main text for abbreviations). The second panel illustrates the amino acid sequence of the DBD with two C4 zinc-fingers and the D domain with the hinge region. The numbering is according to the full length receptor. Residues in red, pink, blue, and green indicate the P-box, D-box, T-box, and A-box, respectively. Solid lined boxes indicate α-helical segments, dashed lines indicate disordered regions. The figure is modified from Moll *et al.* (2006) and Meinke and Siegler (1999) .

The nuclear receptor NGFI-B is constitutively expressed in most tissues (Watson and Milbrandt, 1990), and is induced by multiple cell stimuli, including growth factors such as epidermal growth factor (EGF) (Moll *et al.*, 2006). NGFI-B is frequently over-expressed in cancer cells, which have an unrestricted expression of growth factors. This over-expression might confer a proliferative advantage for tumor cells, as NGFI-B is able to promote cell growth. Ectopic expression of NGFI-B in lung cancer cells mediates its growth-promoting activities through transcriptional regulation of genes (Kolluri *et al.*, 2003). A survival function of NGFI-B has also been demonstrated *in vivo* in the central nervous system (Zetterstroum *et al.*, 1997). However, in response to apoptotic stimuli, NGFI-B is known to have an apoptotic effect in a number of cell types, including cancer cells and neurons (Jacobs *et al.*, 2004; Li *et al.*, 1998). NGFI-B induces apoptosis (section 1.4.3) in a transcription-independent manner by translocating from the nucleus to mitochondria (Li *et al.*, 2000). NGFI-B has no mitochondrial-targeting sequences, but binds via the LBD to the amino-terminal loop region of B-cell lymphoma protein 2 (Bcl-2) in the outer

mitochondrial membrane. The resulting conformational change of Bcl-2 converts it from a protector to a killer (Figure 1.2), triggering cytochrome *c* and apoptosis-inducing factor (AIF) release, and thereby apoptosis (Lin *et al.*, 2004).

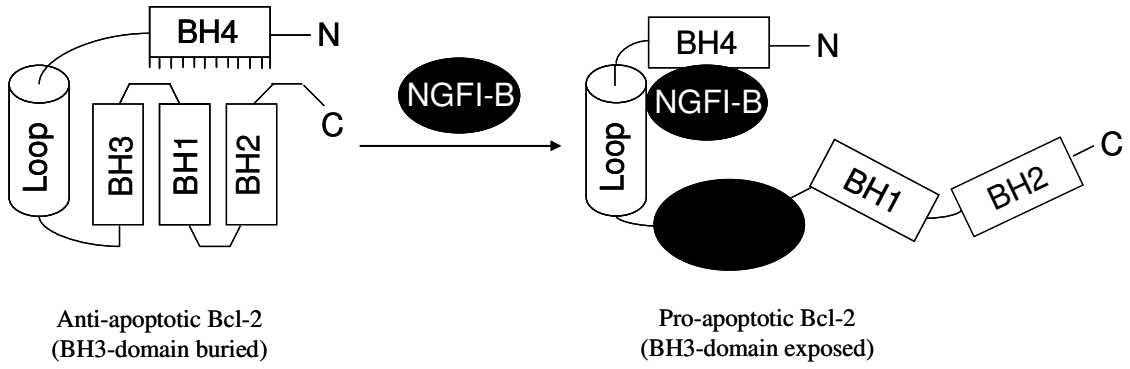

Figure 1.2: Bcl-2 conversion by NGFI-B.
The conformation of anti-apoptotic Bcl-2 is preserved by the Bcl-2 homology (BH) 3 domain-binding hydrophobic pocket involving the carboxyl-terminal region of Bcl-2. Binding of NGFI-B to the Bcl-2 loop interrupts the hydrophobic pocket, and the BH3 domain is exposed. The latter Bcl-2 conformation is pro-apoptotic. The figure is modified from Zhang *et al.* (2007).

X-ray crystallography studies of the putative ligand binding site of NGFI-B revealed a closed conformation that would be inaccessible to ligands (Flaig *et al.*, 2005). This suggests that the *in vivo* activity of NGFI-B is not ligand regulated. However, conclusion should not be drawn based solely on these findings, as the transactivation of closely related Nor-1 was found to be regulated by the direct binding of prostaglandin A2 to the LBD (Kagaya *et al.*, 2005). Two possible mechanisms for ligand independent regulation of NGFI-B is transcriptional activation by a variety of signals, including mitogens, and post-translational modifications, such as phosphorylations (Wingate and Arthur, 2006). NGFI-B is heavily phosphorylated in a various of cell types in response to a number of stimuli (Davis *et al.*, 1993; Fahrner *et al.*, 1990; Han *et al.*, 2006; Hazel *et al.*, 1991; Wingate *et al.*, 2006; Woronicz *et al.*, 1995). The phosphorylations are mainly localized in the A/B region, where 30 % of the amino acids are potential phosphorylation sites (Moll *et al.*, 2006). Deletion of 152 amino acids from the N-terminal completely abolished mitochondrial association of NGFI-B in response to apoptotic stimuli (Li *et al.*, 2000). The phosphorylation of serine 139 (105 in the mouse homologue Nur77), in the AF-1 domain has been implicated in a growth factor dependent nucleocytoplasmic shuttling of NGFI-B (Kang *et al.*, 2000). Jun N-terminal kinase (JNK) phosphorylates an unknown residue in the A/B domain of NGFI-B and increase nuclear export and promote apoptosis (Han *et al.*, 2006; Kolluri *et al.*,

2003). Another phosphorylation site in the amino terminus is threonine 142, which is phosphorylated by extracellular signal-regulated kinase 2 (ERK2) (Slagsvold *et al.*, 2002) (section 1.3). The activity of the mitogen-activated protein (MAP) kinase (MAPK) ERK2 is important in determining whether a cell survives or undergoes apoptosis (Chang *et al.*, 2003). Phosphorylation of NGFI-B by the serine/threonine protein kinase Akt at serine 350, a site within the A box, inhibits DNA binding and transactivation (Hirata *et al.*, 1993; Masuyama *et al.*, 2001; Pekarsky *et al.*, 2001).

NGFI-B has three functional nuclear export signals (NES) in the ligand-binding domain (residues 408-417, 467-476, and 520-530), and two functional nuclear localization signals (NLS) within the DNA binding domain. NLS1 is located within the second zinc finger domain (residues 278-283), while NLS2 is found within the A box (residues 308-313) (Hsu *et al.*, 2004). The presence of the NESs and NLSs suggests that NGFI-B could be transported through nuclear pore complexes (NPCs) via the classical transport pathway (section 1.2).

In summary, the nuclear receptor NGFI-B is capable of promoting both cell death and survival depending on the stimuli. The subcellular localization of NGFI-B is essential for its biological effects, since it functions in the nucleus to induce gene regulation and proliferation, and on the mitochondria to induce apoptosis. This suggests that NGFI-B might be a molecular target for the development of anticancer drugs that induce translocation of NGFI-B from the nucleus to mitochondria in order to inhibit growth and to induce apoptosis (Kolluri *et al.*, 2003). Contrarily, agents that inhibit translocation of NGFI-B to the mitochondria would possibly prevent the cell death of neurons in neurodegenerative disorders.

1.2 Nucleocytoplasmic Transport

Selective transport between the nucleus and the cytoplasm is essential to sustain a distinctive composition of the two compartments. Regulation of the nucleocytoplasmic transport enables proteins, such as NGFI-B, to have divergent functions depending on the subcellular localization.

The bidirectional transport of macromolecules between the cytoplasm and the nucleus occurs through large, multiprotein structures named nuclear pores complexes (NPCs). Ions and small proteins (<40 kDa) can passively diffuse through NPCs, while passage of larger molecules are restricted to those having an NLS or NES. Several classes of NLS and NES exists and are recognized by components of separate pathways (Stewart, 2007). Different nuclear transport pathways imports or exports a specific range of macromolecules, but share many common features based on a series of protein interactions in which cargoes are recognized, translocated through NPCs, and released. The best understood pathway of nucleocytoplasmic transport is the classical nuclear import pathway (Figure 1.3), but alternative mechanisms are likely to exist (Lange *et al.*, 2007). In the classical nuclear import pathway, a protein is imported by a heterodimeric import receptor consisting of importin β and importin α. Importin β mediates interactions with the nuclear pore complex, while the adaptor protein importin α directly binds the NLS (Gorlich *et al.*, 1995). The classical NLSs contain one or two clusters of basic residues (Dingwall and Laskey, 1991; Robbins *et al.*, 1991). Classical nuclear transport requires energy that is provided by a small Ras-family GTPase, Ran, which cycles between a GTP- and a GDP-bound state (Bourne *et al.*, 1990; Quimby and Dasso, 2003). Import receptors bind cargo in the cytoplasm in the absence of RanGTP and release cargo in the nucleus upon RanGTP binding (Figure 1.3) (Smith *et al.*, 2002).

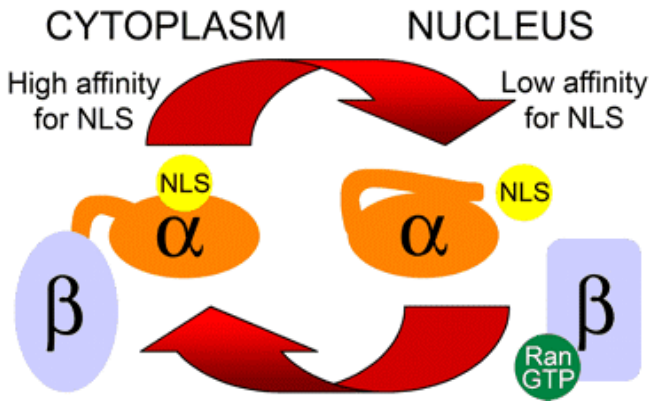

Figure 1.3: The classical nuclear import cycle.
Importin β is bound to the flexible autoinhibitory domain of importin α in the cytoplasm, thereby preventing the autoinhibitory domain from binding the NLS-binding pocket. NLSs are then able to bind to importin α with high affinity. When RanGTP binds to importin β in the nucleus, the resulting conformational change leads to release of the autoinhibitory domain, which now can compete for binding to the NLS-binding pocket. This competition contributes to a low affinity of the NLS for importin α in the nucleus, and NLS cargo delivery is facilitated.
The figure is from Lange *et.al* (2007).

1.3 The MAPK/ERK Kinase (MEK)/ ERK Pathway

The MEK/ERK cascade (Figure 1.4) couples signals from cell surface receptors to transcription factors, and is known to phosphorylate the nuclear receptor NGFI-B (section 1.1) (Slagsvold *et al.*, 2002). Depending upon the stimulus and cell type, this pathway can transmit signals resulting in the prevention or induction of apoptosis (Chang *et al.*, 2003).

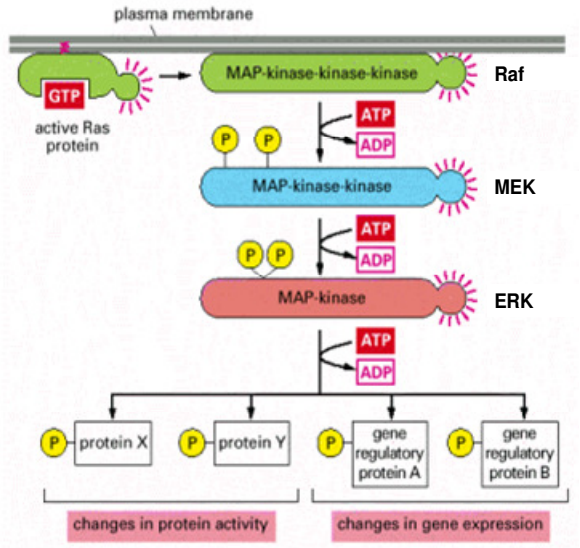

Figure 1.4: The MEK/ERK pathway.
The pathway activated by extracellular signaling via Ras begins with the MAP-kinase-kinase-kinase RAF, which activates the MAP-kinase-kinase MEK. MEK triggers the activation of the MAPK ERK by phosphorylating a threonine and a tyrosine in its activation loop. ERK phosphorylates numerous substrates at serine and threonine residues in all cell compartments. In the nucleus, ERK may phosphorylate transcription factors and thereby activate the transcription of immediate early genes. The resulting changes in gene expression and protein activity cause complex changes in cell behavior (Chang *et al.*, 2003). The figure is modified from Alberts *et al*. (2002).

The MAP kinase ERK is of great importance in the control of cell growth and differentiation, and is also involved in neuronal plasticity. Glutamate (section 1.4.1) activation of the MEK/ERK pathway via the *N*-methyl-d-aspartate receptor (NMDAR) (section 1.4.2) is involved in mammalian memory and learning (Bading and Greenberg, 1991; Kurino *et al.*, 1995; Mao *et al.*, 2004; Perkinton *et al.*, 2002; Platenik *et al.*, 2000). However, the ERK activation during neuropathological over-stimulation of NMDARs may contribute to neuronal death in the adult brain (Jiang *et al.*, 2000). The relevance of MEK/ERK pathways in neuronal cell survival was documented in PC12 pheochromocytoma cells where down-regulation of ERK mediated by NGF withdrawal led to apoptosis, whereas the activation of the ERK signaling pathway by NGF inhibited apoptosis (Xia *et al.*, 1995b). Another growth factor, EGF, reduces the glutamate-induced neuronal death in cerebellar granule neurons (CGN) (section 1.5.1) from fetal rats, as well as in other neuronal cells (Abe and Saito, 1992; Casper and Blum, 1995; Gunn-Moore and Tavare, 1998). EGF is shown to activate ERK2, and to inhibit apoptosis-induced translocation of NGFI-B from the nucleus to the mitochondria (Jacobs *et al.*, 2004).

1.4 Glutamate-Induced Excitotoxicity

The nuclear receptor NGFI-B is highly expressed in adult neurons and is shown to translocate to mitochondria in glutamate-exposed cerebellar granule neurons (CGN) (Jacobs *et al.*, 2004).

1.4.1 Glutamate as a Neurotoxin

The amino acid $_{L}$-glutamate is the principal excitatory neurotransmitter in the mammalian brain (reviewed in (Fonnum, 1984) where it is involved in plasticity, memory, and learning (Asztély and Gustafsson, 1996; Maren and Baudry, 1995). Fifty years ago, it was shown that excessive extracellular levels of glutamate for prolonged periods caused cell death (Lucas and Newhouse, 1957). Excitotoxicity refers to the phenomenon in which over-activity of receptors responding to excitatory neurotransmitters injure neurons, and results in cell death (Olney, 1969). Death of adult neurons will induce irreversible damages, as the remaining cells will not have the ability to regenerate and compensate the loss. Excitotoxicity has been implicated in the pathogenesis of human neurodegenerative disorders such as Parkinson's, Huntington's, and Alzheimer's diseases (Gardoni and Di Luca, 2006).

Glutamate activates two families of receptors, namely the metabotropic receptors that are linked to G-proteins and second messenger signaling, and the ionotropic receptors that are ligand-gated ion channels. Among the latter are three subclasses designated by their selective agonists: kainic acid receptors, α-amino-3-hydroxy-5-methyl-4-isoxazolepropionic acid (AMPA) receptors, and NMDARs (Chen and Wyllie, 2006). NMDARs exhibit high permeability to calcium and a relatively slow rate of desensitization and deactivation, and, consequently, play a more prominent role in mediating excitotoxicity than the other glutamate receptors (Choi *et al.*, 1988; Paoletti and Neyton, 2007).

1.4.2 NMDAR-Mediated Neuronal Injury

The NMDARs are heteromultimeric complexes of the subtypes NR1, NR2 and NR3. There are eight different NR1 subunits generated by alternative splicing from a single gene, four different NR2 subunits (A, B, C and D) and two NR3 subunits (A and B); the NR2 and NR3 subunits are encoded by six separate genes (Dingledine *et al.*, 1999; Nishi *et al.*, 2001; Sucher *et al.*, 1995).

The consensus stoichiometry of NMDARs is that they are tetramers usually incorporating two NR1 and 2 NR2 subunits of the same or different subtypes (Dingledine *et al.*, 1999). Such NMDARs requires the binding of both glutamate and the co-agonist glycine to be activated (Johnson and Ascher, 1987). Glycine binds to NR1 subunits while glutamate binds to NR2A-D subunits (Kuryatov *et al.*, 1994; Laube *et al.*, 1997). Mg^{2+} that is bound to a separate site in the receptor will loose its affinity when the neuron depolarizes, and the channel opens for ion flow (Figure 1.5) (Mori *et al.*, 1992). In cells expressing NR3, this subunit will co-assemble with NR1 and NR2 and form ternary NR1/NR2/NR3 tetrameric complexes (Sasaki *et al.*, 2002).

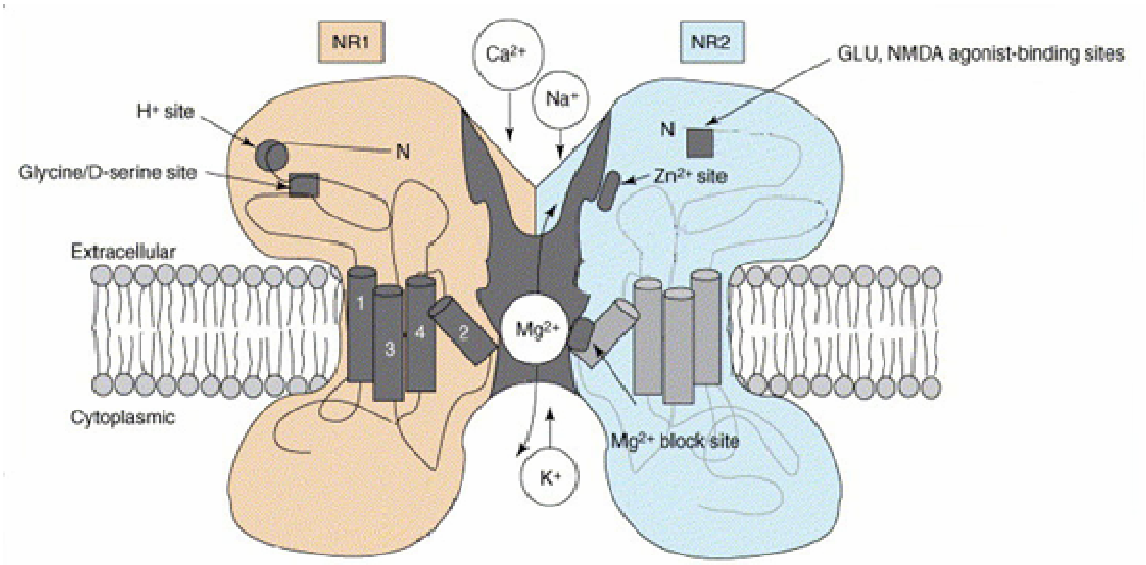

Figure 1.5: NMDA receptor organization.
Schematic presentation of the NMDA receptor with overlaid tertiary structures for the NR1 and NR2 subunits and N-terminal binding sites for glycine and glutamate. The figure is modified from Kristiansen *et al.* (2007).

NMDAR-induced neuronal injury after prolonged exposure to glutamate will result from a massive influx of Ca^{2+} that trigger mitochondrial dysfunction, generation of reactive oxygen species (ROS), and cell death. The composition of NMDAR subunits affects neuronal vulnerability to glutamate. Changes in the relative expression levels and/or location of the NR2A and NR2B subunits is involved in the increased excitotoxicity acquired with age of neurons in culture (Brewer *et al.*, 2007).

1.4.3 Intrinsic Apoptotic Pathways Involving Mitochondria

A mild insult of glutamate toxicity will initiate neuronal apoptosis, while stronger insults results in necrosis. Apoptosis (Kerr *et al.*, 1972) is associated with cell membrane blebbing, cell shrinkage, nuclear and cytoplasmic condensation, and DNA fragmentation and condensation. Finally, the cell is engulfed by macrophages and neighboring cells, thereby avoiding damage of the surrounding tissue. In contrast to the tightly organized process of apoptosis, necrosis is characterized by cell swelling, severe mitochondrial damage, and eventually cell lysis. Rupture of the cell will release intracellular contents that potentially could cause a damaging inflammatory response. Neurotransmitters can also be released, causing excitotoxicity to neighboring cells (Fink and Cookson, 2005). Regardless of differing morphology does apoptosis and necrosis have numerous cellular mechanisms in common, which led to the proposal of the apoptosis-necrosis continuum model (Proskuryakov *et al.*, 2003; Zeiss, 2003).

Apoptotic stimuli leads to the release of pro-apoptotic proteins that reside in the inter-membrane space of mitochondria to the cytosol (Armstrong, 2006). The permeabilization of the outer mitochondrial membrane is normally prevented by Bcl-2 and several other members of the Bcl-2 family of proteins. The regulatory effect of Bcl-2 on membrane permeability is due to the presence of four conserved sequence motifs known as Bcl-2 homology (BH) domains (Figure 1.2) (Chan and Yu, 2004). Apoptogenic proteins, such as NGFI-B (section 1.1), can inactivate Bcl-2, resulting in the generation of pores that permeate the mitochondrial outer membrane (Figure 1.6) (Lin *et al.*, 2004). The released proteins can propagate apoptosis either by activating a group of enzymes of the cysteine protease family known as caspases, or by acting in a caspase-independent fashion. Caspase dependent factors include cytochrome *c*, a small heme-containing protein involved in electron transport and oxidative phosphorylation. Cytochrome *c* released to the cytoplasm will combine with a highly conserved protein known as apoptotic protease-activating factor 1 (Apaf-1) and induce the ATP-dependent formation of an oligomeric complex known as the apoptosome (Cain *et al.*, 2002). The apoptosome recruits and processes the crucial initiator caspase, caspase 9, which cleaves and activates downstream caspases, such as the effector caspase 3 (Jiang and Wang, 2000). The effector caspases will subsequently cleave a variety of cellular proteins, and thereby activate or inactivate them. These proteins will be

directly or indirectly responsible for the morphological and biochemical alterations in the apoptotic cell (Gogvadze and Orrenius, 2006).

The mitochondrial flavoprotein AIF is the main mediator of caspase-independent apoptosis (Vahsen *et al.*, 2004). AIF has a NADH oxidase activity and might participate in scavenging of reactive oxygen species (ROS) (Klein *et al.*, 2002). Upon apoptosis, AIF translocates from the mitochondria to the nucleus where it participates in chromatin condensation and DNA fragmentation (Susin *et al.*, 1999).

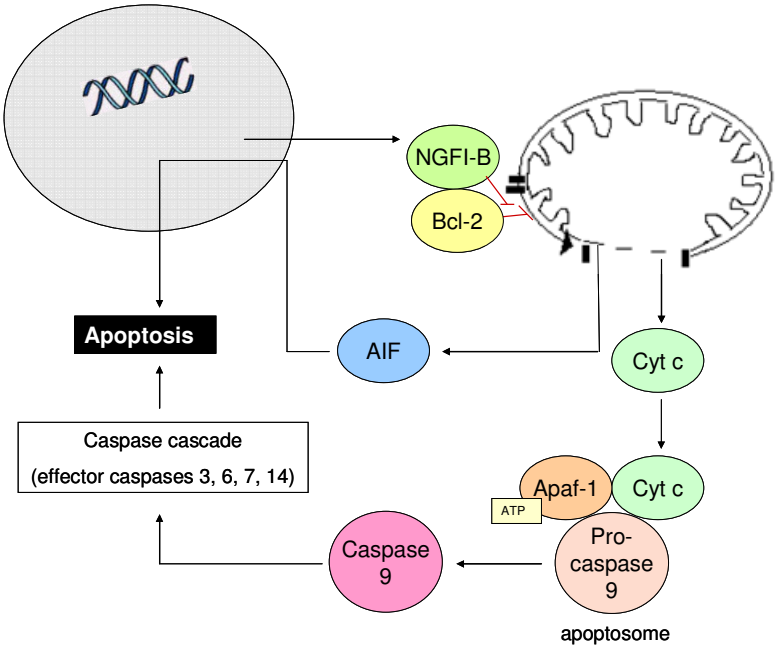

Figure 1.6: Mitochondrial apoptosis. NGFI-B translocates from the nucleus to the mitochondria in response to apoptotic stimuli. The resulting conformational change of anti-apoptotic Bcl-2 makes it pro-apoptotic. As a result, cytochrome *c* and AIF are released and apoptosis is induced (see text for details).

1.5 Introduction to Experimental Systems

1.5.1 Cerebellar Granule Neurons as an *In Vitro* Model for Neuronal Apoptosis

Primary cultures of cerebellar granule neurons (CGN) are a popular *in vitro* model for studying neuronal apoptosis, as well as other aspects of neurobiology, in a very uniform population of neurons (95-98 % pure neuron cultures) (Figure 1.7) (Ciani and Paulsen, 1995). Glutamate (section 1.4.1) efficiently induces apoptosis in cultured CGN, which express all of the glutamate receptor subtypes including the NMDA receptor (section 1.4.2). The CGN express AIF (section

1.4.3), and translocation of NGFI-B (section 1.1) from the nucleus to the mitochondria has been demonstrated in this cell model (Jacobs *et al.*, 2004).

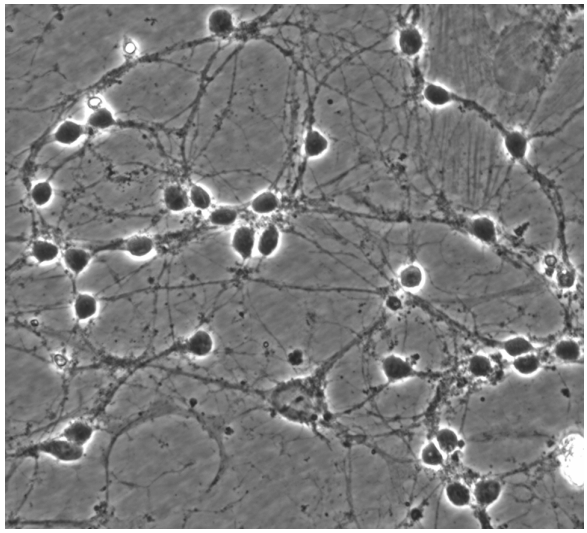

Figure 1.7: Phase contrast micrograph of 14 days old untreated CGN.

The cell bodies of CGN are located in the deepest layer of the tri-laminar cerebellar cortex with axons protruded up into the superficial molecular layer. The CGN are the largest homogenous neuronal population in the mammalian brain, constituting more than 90 % of the neurons in the cerebellum (Contestabile, 2002). The neurogenesis of granule cells is mainly postnatal, making them a suited source for primary neurons to be grown *in vitro*. In culture, the CGN will get altered connectivity by forming synapses with each other. This feature makes the CGN suitable for studies of neuronal toxicity in general, not only cerebellar toxicity. Glutamate toxicity peaks in CGN that have been maintained for 14 days *in vitro*, due to changes in the composition of NMDAR subtypes (section 1.4.2) (Xia *et al.*, 1995a). As the CGN cultures mature, there is a shift between high expression of the NR2C subunit to a more predominant expression of NR2A and NR2B (Gerber and Vallano, 2006).

The advantage of using CGN primary cultures instead of cell lines is that a primary culture has cells that are more similar to the cells *in vivo.* However, a disadvantage is that the CGN show low transfection efficiency (Ciani and Paulsen, 1995). Furthermore, microscopic examination of subcellular distributions within CGN are demanding, as the cells have nuclei that encompass most of the cell body, leaving a thin rim of cytoplasm.

1.5.2 CV-1 cells

The CV-1 cell line was established in the early1960s from the kidney tissue of an adult male African green monkey (*Cercopithecus aethiops*) (Hopps *et al.*, 1963). This cell line express NGFI-B, grows adherently to glass or plastic surfaces, and is easily transfected. The cells have a distinct nucleus and a large cytoplasm, and are therefore well suited for microscopic experiments studying protein distribution within cells.

1.5.3 The Firefly Luciferin/Luciferase Reaction

The luciferin/luciferase reaction is widely used as a sensitive method for monitoring intracellular ATP concentration. Luciferase from *Phontinus pyralus*, the most common species of North American fireflies, catalyze the formation of D(-)-luciferyl adenylate from D(-)-luciferin and ATP-Mg. The oxidation of the acyl adenylate by molecular oxygen leads to the formation of an enzyme bound product molecule in the excited state, which subsequently decays to the ground-state oxyluciferin with the emission of light (Seliger *et al.*, 1961). When ATP is the limiting factor in the luciferin oxidation reaction, the amount of light produced is proportional to the ATP concentration of the sample (Allue I, 1996).

1.6 Aims of the Thesis

1. To establish a luminometric ATP-assay with over-expressed luciferase from CV-1 cells for validation of ATP-depletion in these cells.
2. To determine whether nuclear import of NGFI-B in CV-1 cells is energy-dependent.
3. To investigate the effect of a threonine 142 to alanine or glutamate mutation on the nuclear import of NGFI-B in CV-1 cells, and whether the nuclear import of NGFI-B is influenced by over-expression of dominant active or dominant negative ERK2.
4. To examine the effect of MEK/ERK inhibition before and after glutamate exposure on CGN death.
5. To investigate whether CGN is a suitable model for determination of neuronal NGFI-B traffic for studies using a confocal microscope.

2 Materials and Methods

2.1 CV-1 Cells

2.1.1 Splitting CV-1 Cells

CV-1 cells were grown in 175 cm^2 flasks and were incubated at 37 ºC in 5 % CO_2. Cells were split when confluent every 3 or 4 days.

Splitting procedure:

1. Remove medium.
2. Wash with 2 ml trypsin-ethylenediaminetetraacetic acid (EDTA).
3. Add 2 ml trypsin-EDTA and incubate at 37 ºC in 5 % CO_2 for 10 min.
4. Tap the flask and add 10 ml CV-1 medium (Table 2.1).
5. Mix and dispense 1.5 ml cell suspension into culture flasks containing 20 ml CV-1 medium.

Table 2.1: CV-1 cell culture medium with fetal bovine serum

Component	Quantity
Fetal bovine serum (FBS)	50 ml
Sodium pyruvate (from 100x stock)	5 ml
Penicillin-Streptomycin (from 100x stock)	5 ml
Dulbecoos MEM (DMEM)	500 ml

2.1.2 Transient Transfection of CV-1 Cells

CV-1 cells were seeded at 5.4 x 10^3 cells / cm^2 into culture dishes (21.5 cm^2) to a volume of 3.3 ml for later harvesting (section 2.1.4), and at 2.1 x 10^4 cells / cm^2 into 4 well chambered cover glasses (1.7 cm^2) to a volume of 1 ml for fluorescence recovery after photobleaching (FRAP) experiments (section 2.1.5). The cells were transfected by calcium phosphate precipitation (Graham and van der Eb, 1973) one day after seeding.

Transfection procedure:

1. Mix equal amounts of N,N-bis-(2-hydroxyethyl)-2-aminoethanesulfonic acid (BES) buffered saline solution (BBS) (Table 2.2) and 0.25 M $CaCl_2$ (in distilled water filter sterilized (0.2µm)).
2. Add 10 µg DNA/ml (Table 2.3).
3. Whirlmix 5+10 s and incubate for 20 min at room temperature.
4. Add drop-wise 330 µl to culture dishes and 100 µl to 4 well plates.
5. Incubate at 37 ºC with 5 % CO_2 for two days (section 2.1.3 and 2.1.5).

Table 2.2: BBS

Component	Final concentration	Quantity
BES	50 mM	5.333 g
Na_2HPO_4	2 mM	0.134 g
NaCl (5 M)	280 mM	28.0 ml
MQ-H_2O		ad 500 ml

pH was adjusted to 6.75, 6.85, 6.95, 7.00, and 7.05 with NaOH and HCl. Solutions were filter sterilized (0.2 µm) and the most efficient BBS pH was determined by transfection and luciferase measurements (Moen, 2007).

Table 2.3: Plasmids for transfections

Gene product	Plasmid	Source	Plasmid short name	FRAP	ATP-assay
firefly luciferase	prsv-luciferase	Promega	rsv-luc		1 µg/ml
green fluorescent protein (GFP)	pAd-GFP	Kindly provided by Prof. Anne Carine Østvold, University of Oslo	GFP	3 µg/ml	
GFP-tagged NGFI-B	pNGFI-B-GFP	Jacobs *et.al* (2004)	NGFI-B-GFP	3 µg/ml	
GFP-tagged T142A-NGFI-B	pNGFI-B(T142A)-GFP	Produced in the Prof. R.E. Paulsen laboratory	NGFI-B-T142A-GFP	3 µg/ml	
GFP-tagged T142E-NGFI-B	pNGFI-B(T142E)-GFP	Produced in the Prof. R.E. Paulsen laboratory	NGFI-B-T142E-GFP	3 µg/ml	
ERK2 *dominant active*	pCMV5 ERK2-MEK 1R4F	Kindly provided by Dr. M. Cobb, University of Texas	MEKERK2	5 µg/ml	
ERK2 *dominant negative*	pCMV5 ERK2 K52R	Kindly provided by Dr. M. Cobb, University of Texas	KRERK2	5 µg/ml	
none (empty expressor plasmid)	pCMV neo	Wilson *et.al* (1991)	CMV	2 µg/ml or 7 µg/ml	9 µg/ml

Cells for ATP measurements (section 2.1.3) were transfected with the plasmids rsv-luc and CMV. Cells for FRAP experiments (section 2.1.5) were transfected with GFP, NGFI-B-GFP, NGFI-B-T142A-GFP, or NGFI-B-T142E-GFP. Certain NGFI-B-GFP-transfected cells were treated with EGF (5 ng/ml) for 10 min before FRAP. NGFI-B-T142A-GFP and NGFI-B-T142E-GFP had replaced the threonine 142 residue in NGFI-B-GFP with alanine or glutamate, respectively, and was made by replacing nucleotides 510-695 of NGFI-B-GFP with the corresponding mutated nucleotide sequence from pNGFI-B-T142A and pNGFI-B-142E (Slagsvold *et al.*, 2002). The threonine-to-alanine mutation was expected to mimic the dephosphorylated state of the residue, whereas the mutation to glutamate could mimic constitutive phosphorylation. Certain cells were also co-transfected with MEKERK2 (dominant (constitutive) active) or KRERK2 (dominant negative (inactive)). CMV was added to obtain a final concentration of 10 µg DNA/ml.

2.1.3 ATP-Depletion

Cells for ATP measurements (section 2.1.4) and FRAP (section 2.1.5) experiments were ATP-depleted two days after transfection. NaN_3 was added to inhibit cytochrome *c* oxidase in the electron transport chain, and cells were depleted of glucose to abolish glycolysis.

ATP-depletion procedure:

1. Aspirate CV-1 medium from culture dishes.
2. Wash with, and add, 3.3 ml glucose-free CV-1 medium.
3. Add NaN_3 from a 0.3 M stock to a final concentration of 5 mM.
4. Incubate for 2, 4, or 6 hrs at 37 ºC in 5 % CO_2.

2.1.4 Cell Harvest and ATP-Measurement

Untreated or ATP-depleted non-transfected cells and cells transfected with rsv-luc were harvested, and ATP was measured, 2 days after transfection.

Harvesting procedure:

1. Wash dishes twice with ice-cold phosphate buffered saline (PBS) (Table 2.15).
2. Add 235 µl 0.1 % LUC with freshly added 0.5 M Dithiothreitol (DTT) (500:1) (Table 2.4), and incubate for 5 min at room temperature.
3. Scrape off cells with a cell lifter and transfer to eppendorf tubes on ice.
4. Centrifuge for 5 min at 16 000 x g at 4 ºC.
5. Place tubes back on ice.

The following exceptions were made from the harvesting procedure (listed in section 3.1):

- Cells were harvested in 235 µl of boiling Milli Q (MQ)-H_2O. The boiling water would lyse cells and denature proteins (Yang *et al.*, 2002).
- Solutions in the harvesting procedure were added trichloroacetic acid (TCA) to a concentration of 10, 5, 2.5, or 1.25 % (Berg-Johnsen *et al.*, 1993), and cells were harvested. TCA is usually added to EDTA when used in protein precipitation. However, EDTA was not added because of its ability of to form complexes with Mg^{2+}, which is required for the luciferin oxidation reaction.
- Cell lysates were boiled for 15 min to denature proteins, and tubes were placed back on ice.

Table 2.4: Cell harvest solutions

Solution	Component	Final concentration	Quantity
DTT stock	DDT	500 mM	77.2 mg
	MQ-H_2O		1.0 ml
0.1 % LUC	1 M trishydroxymethylaminomethane (Tris) adjusted to pH 7.8 with 1 M 2-(*N*-morpholino)ethanesulfonic acid (MES)	50 mM	5.0 ml
	Triton X-100	0.1 %	0.1 ml
	MQ-H_2O		ad 100 ml

ATP was measured as relative luciferase units (RLU) using an EG&G Berthold Lumat LB9507 luminometer. To a 5 ml Sarstadt tube, 10 µl cell lysate supernatant from cells transfected with rsv-luc, and thereby expressing luciferase, and 140 µl of LUC-cocktail with no ATP were added to 50 µl of ATP-dilution (Table 2.5) or cell lysate supernatant from non-transfected cells. The tube was inserted in the luminometer, luciferin (Table 2.5) was dispensed (100 µl), and the emission of light was measured for 2 sec. A sample containing 10 µl cell lysate from luciferase transfected cells and 190 µl LUC-cocktail without ATP was measured as a negative control.

Table 2.5: Solutions for ATP-measurements

Solution	**Component**	**Final concentration**	**Quantity**
Luciferin	Luciferin	1 mM	30.0 mg
	MQ-H_2O		100 ml
LUC-cocktail	ATP	4 mM	240.0 mg
	1 M $Mg(CH_3COO)_2$	20 mM	2.0 ml
	1 M Tris adjusted to pH 7.8 with 1 M MES	83 mM	8.3 ml
	MQ-H_2O		ad 100 ml
LUC-cocktail with no ATP was also prepared. A 10-fold dilution series of the LUC-cocktail in LUC-cocktail with no ATP was made.			

2.1.5 Fluorescence Recovery after Photobleaching (FRAP) Experiments

FRAP was developed in the 1970s by Axelrod and coworkers (Axelrod *et al.*, 1976) and is a popular technique for investigating the mobility of proteins in living cells. By using a confocal laser-scanning microscope (CLSM), fluorescent molecules are photobleached in an area by a high-powered focused laser beam in FRAP experiments. The photobleached molecules lose their ability to emit fluorescence when exposed to repeated cycles of excitation and emission. Subsequent diffusion of surrounding non-bleached fluorescent molecules into the bleached area leads to a recovery of fluorescence, which is recorded at low laser power.

CV-1 cells for FRAP experiments were split into 4 well chambered cover glasses (section 2.1.1), transfected (section 2.1.2), and incubated for 2 days. The FRAP analysis was performed at room temperature with a Nikon C-1 confocal unit mounted on a TE 2000E inverted microscope run by EZ-C1 3.40 software with a 60x oil immersion objective. Cells were imaged with the 488 nm laser power set to minimum and 1.5 amps, with a small pinhole. Gain was set between 4.40 and 6.05 so that no pixels were saturated because some information is lost in saturated pixels. The pre-bleach image was used as a reference for the steady-state distribution of florescent molecules. Next, the cell nucleus was outlined and bleached by 15 repeated scans with the 488 nm laser power at 100 % and 8 amps and the pinhole set to open. After bleaching, the laser power was reset to pre-bleach values and the pinhole to small, and one image was taken of the whole cell every 22 seconds, to a total of 30 images. The images were analyzed in the EZ-C1 3.20 FreeViewer software to obtain pixel intensity values in analog-to-digital converter units (ADC-units).

2.2 Culture of Rat Cerebellar Granule Neurons

Cerebellar granule neurons (CGN) were derived from 7 days old Wistar rats from Charles River Laboratories, Germany. CGN primary cultures are widely used to investigate the neurotoxic effects of various factors, and they have provided important information concerning mechanisms of cell death (Vaudry *et al.*, 2003). The CGN requires chronic depolarization conditions to survive, and this is obtained by raising potassium concentrations from the *in vivo* concentration of 3.5-5.5 mM to >20 mM (Gallo *et al.*, 1987). This state of sustained excitation is believed to mimic *in vivo* conditions related to the formation of excitatory synapses from mossy fibers (one of the major inputs to the cerebellum) onto differentiating CGN (Contestabile, 2002). CGN cultures were prepared according to a modified version of the procedure by Gallo *et al.* (1987) (section 2.2.1-2.2.3).

2.2.1 Coating of Culture Dishes with Poly-L-Lysine

To obtain a better adhesion of the CGN to the culture dishes, the dishes were coated with poly-L-lysine one day prior to preparation.

Coating procedure:

1. Remove 10 ml from a 500 ml bottle of autoclaved MQ water and transfer to a sterile bottle of poly-L-lysine (5 mg).
2. Dissolve and transfer back into the 500 ml bottle.
3. Put 4 cover glasses into culture dishes for CLSM imaging.
4. Dispense 2 ml/ culture dish (21.5 cm^2).
5. Coat 10 culture dishes per 3 rat brains.
6. Aspirate fluid after 30-60 min and allow drying over night.

2.2.2 CGN Preparation

CGN preparation procedure:

Required equipment was given in Table 2.6. The given amounts are for preparation of cell cultures derived from 40-80 rats.

1. Transport the heads of decapitated rat pups to LAF-hood.
2. Isolate cerebella with scissors and tweezers and transfer to a large petri dish containing solution 1 (Table 2.7).
3. Remove meninges with tweezers and transfer cerebella to another large petri dish containing solution 1.
4. Remove solution 1 and cut cerebella in two directions at right angles to each other with a scalpel.
5. Add 10 ml solution 1 and transfer cerebella to a tube containing another 10 ml of solution 1. Centrifuge at 170 x g for 0.5 -1 min.
6. Remove supernatant and resuspend pellet in 10 ml solution 2 (Table 2.7).
7. Transfer cell suspension to a trypsination bottle and tighten cap loosely. Keep in a 37 ºC shaking water bath for 15 min.
8. Collect cerebellar pieces with a Pasteur pipette and transfer to a tube containing 14 ml solution 4 (Table 2.7). Add solution 4 to a final volume of 50 ml and centrifuge at 170 x g for 2 min.
9. Remove supernatant and add the volume of 3 Pasteur pipettes of solution 3 (Table 2.7). Narrow the tip of a Pasteur pipette by passing it through a flame. Dissolve pellet carefully by pipetting 20 times up and down with the Pasteur pipette. Allow aggregates to settle for a few minutes.
10. Remove upper part of the solution (free of clumps) and transfer to a tube containing 15 ml solution 5 (Table 2.7).
11. Add 2 ml solution 3 to remaining cerebellar pieces and repeat step 10, making a narrower opening in the Pasteur pipette.
12. If necessary, repeat steps 9-11.
13. Centrifuge cell suspension at 140 x g for 7 min.

14. Remove supernatant and resuspend pellet in 10 ml cell culture medium with fetal bovine serum (Table 2.9). Transfer into a flask containing half of the calculated amount of medium. Remove 0.5 ml of cell suspension for cell count in a Bürcher chamber. Calculate the quantity of the medium to be added. The desired cell density is 1.2 x10^6 cells/ml.
15. Mix well and distribute 3.3 ml per culture dish.
16. Incubate at 37 ºC with 5 % CO_2 for 7 days.

Equipment was sterilized in the autoclave for 20 min at 121 ºC.

Table 2.6: Equipment

1 pair of scissors and 2 tweezers for dissection
2 tweezers for removing of meninges
6 Pasteur pipettes with filter
1 trypsination bottle
Glass bottles for solutions 1-5 and culture medium
1 scalpel
2 large petri dishes
Three 50 ml plastic tubes

Five solutions (Table 2.7) were freshly made for each preparation of CGN.

Table 2.7: Solutions 1-5

Solution 1	1.50 g Bovine serum albumin (BSA) 4 ml $MgSO_4$ (3.82 g/100 ml) 50 ml Krebs-Ringer solutions 10x (Table 2.8) Distilled water ad 500 ml
Solution 2	25 mg trypsin 100 ml solution 1
Solution 3	0.5 mg $MgSO_4$ (3.82 g/100 ml) 6.25 mg deoxyribonuclease I (DNaseI) 26 mg Trypsin inhibitor Solution 1 ad 50 ml
Solution 4	16 ml solution 3 100 ml solution 1
Solution 5	320 µl $CaCl_2$ (1.20 g/100 ml) 320 µl $MgSO_4$ (3.82 g/100 ml) 40 ml solution 1

The solutions were filter sterilized (0.2 µm).

Table 2.8: Krebs-Ringer solution (10x)

Component	Final concentration	Quantity
Phenol red	0.3 mM	50 mg
KH_2PO_4	10 mM	0.83 g
KCl	50 mM	1.80 g
Glucose	0.14 M	12.85 g
NaCl	1.21 M	35.35 g
$NaHCO_3$	0.25 M	10.70 g
Distilled water		ad 500 ml

Krebs-Ringer solution was stored in a refrigerator, and had a shelf life of 5-6 months.

Table 2.9: CGN culture medium with fetal bovine serum

Component	Final concentration	Quantity
Heat inactivated fetal bovine serum	~10 %	50 ml
Gentamicin sulfate	90.9 µg/ml	50 mg
Glutamine	1.8 mM	146 mg
KCl	25.5 mM	825 mg*
Basal Medium Eagle (BME)		500 ml
	*5.4 mM is already present in the medium	

KCl, glutamine, and gentamicin sulfate were added to 30 ml medium removed from a sterile bottle of 500 ml BME. The solution was filter sterilized (0. 22 µl) back into the bottle. Heat inactivated fetal bovine serum (30 min in 56 ºC water bath) was added.

2.2.3 Prevention of Non-Neuronal Cell Growth

Cytosine β-D-arabino-furanoside (Ara-C) was added to the cultures 16-20 hrs after preparation to inhibit proliferation of non-neuronal cells.

Procedure for adding Ara-C:

Dissolve 1 mg Ara-C in 10 ml cell culture medium with fetal bovine serum and filter sterilize (0.2 µm). Add 83µl/ 21.5 cm^2 dish to obtain the final concentration of 10 µM.

2.3 Exposure of Cultured Cerebellar Granule Neurons

Cultured CGN were incubated with MEK inhibitor U0126 (sections 2.3.1 and 2.3.4) and EGF (section 2.3.2), and exposed to glutamate (section 2.3.3), 7 days after preparation.

2.3.1 Pre-Incubation with MEK Inhibitor U0126

The U0126 stock was added to the culture dishes to a final concentration of 10µM. The dishes were incubated at 37 ºC with 5 % CO_2 for 1 h, followed by glutamate or buffer control exposure.

U0126 stock (10 mM):

Add 234 µl dimethyl sulfoxide (DMSO) to 1 mg U0126. Store at -20 ºC.

2.3.2 Pre-Incubation with Epidermal Growth Factor

The CGN were pre-incubated in a pre-incubation solution consisting of Locke's solution with or without EGF (5 ng/ml).

Cells later exposed to glutamate were pre-incubated in Locke's solution without magnesium (Table 2.10), whereas buffer controls were pre-incubated in Locke's solution with magnesium (Table 2.11).

Pre-incubation procedure:

1. Remove cell medium.
2. Add 1 ml pre-incubation solution, swirl, and aspirate.
3. Add 2 ml pre-incubation solution.
4. Incubate for 15 min at room temperature.

Table 2.10 Locke's solution without magnesium

Component	Final concentration	Quantity
$CaCl_2$	2.3 mM	0.34 g
$NaHCO_3$	3.6 mM	0.30 g
4-(2-hydroxyethyl)-1-piperazineethanesulfonic acid (HEPES) (pH 7.4)	5.0 mM	1.19 g
KCl	5.6 mM	0.42 g
Glucose	5.6 mM	1.00 g
NaCl	154.0 mM	9.00 g
Distilled water		ad 1000 ml

Adjust pH to 7.4.

Table 2.11: Locke's solution with magnesium

Component	Final concentration	Quantity
$MgCl_2$ x $7H_2O$	1.2 mM	0.24 g
Locke's solution without magnesium		1000 ml

2.3.3 Glutamate or Buffer Exposure

After pre-incubation, cells were exposed to glutamate or physiological buffer. Locke's solution with (Table 2.11) or without (Table 2.10) magnesium was used as a physiological exposure buffer.

Exposure procedure:

1. Remove cell medium through aspiration.
2. Add 1 ml exposure solution (Table 2.12), swirl, and aspirate.
3. Add 2 ml exposure solution.
4. Incubate for 15 min at room temperature.
5. Remove exposure solution.
6. Add 1 ml cell culture medium without serum (Table 2.13), swirl, and aspirate.
7. Add 2 ml cell culture medium without serum.
8. Incubate at 37 ºC with 5 % CO_2 for 2 hrs for fixing (section 2.5.1) and immunostaining (section 2.5.2).
9. Incubate at 37 ºC with 5 % CO_2 for 24 hrs for detection of cell death (section 2.4)

Table 2.12: Exposure solutions

10 mM glutamate stock	
Glutamate	1.690 mg
Distilled water	1 ml
Store at -20 ºC	
1 mM glycine stock	
Glycine	0.075 mg
Distilled water	1 ml
Store at -20 ºC	
Glutamate exposure solution	
Lockes solution without magnesium	
Glycine	10 µM
Glutamate	100 µM
Buffer exposure solution	
Lockes solution with magnesium	

Table 2.13: Cell culture medium without serum

Component	Final concentration	Quantity
Gentamicin sulfate	100 µg/ml	50 mg
Glutamine	2 mM	146 mg
KCl	27 mM	825 mg
BME		500 ml

Add KCl, glutamine, and gentamicin sulfate to 30 ml medium removed from a sterile 500 ml bottle of BME. Filter sterilize (0. 22 µm) back into the bottle.

2.3.4 Post-Incubation with MEK Inhibitor U0126

The MEK inhibitor U0126 was added 4 or 6 hrs after glutamate exposure.

Post-incubation procedure:

1. Add U0126 stock to the CGN culture dishes to a final concentration of 10 µM.
2. Incubate at 37 ºC with 5 % CO_2 for 1 h.
3. Add 1 ml cell culture medium without serum, swirl, and aspirate.
4. Add 2 ml cell culture medium without serum.

2.4 Detection of Cerebellar Granule Neuron Death

24 hrs after exposure, dying cells were detected by trypan blue staining. Trypan blue does not traverse the cell membranes of living cells, but is absorbed when the dying cells loose membrane integrity. In consequence, apoptotic and necrotic cells are shown in a distinct blue color under a microscope.

Trypan blue staining procedure:

1. Aspirate cell medium from the dishes until there is 1 ml left in the dish.
2. Add 250 µl trypan blue staining solution (Table 2.14).
3. Incubate at 37 ºC with 5 % CO_2 for 30 min.
4. Remove staining solution.
5. Count stained (dead) and unstained (viable) cells under a microscope.
6. Determine the percentage of dead cells.

Table 2.14: Solutions for trypan blue staining

Trypan blue stock	
Trypan blue	1 g
Distilled water	50 ml
Heat until boiling while swirling. Cool at room temperature and filter. Keep at room temperature.	
NaCl stock	
NaCl	1.8 g
Distilled water	100 ml
Keep at room temperature	
Trypan blue staining solution	
Trypan blue stock (2 %)	125 µl x number of dishes
NaCl Stock (1.8 g/ 100 ml)	125 µl x number of dishes

2.5 Immunofluorescence Staining of Cerebellar Granule Neurons

NGFI-B and AIF in CGN were immunostained with specific primary antibodies followed by fluorescent secondary antibodies for visualization under a CLSM microscope.

2.5.1 Fixing

Cells were fixed 2 hrs after exposure to preserve cells for analysis and storage. Paraformaldehyde (PFA) was used as a protein cross linking fixative.

PFA fixing procedure:

1. Remove cell media from the dishes.
2. Wash with PBS (Table 2.15).
3. Add 2 ml freshly made 4 % PFA in PBS.
4. Incubate at room temperature for 2, 5 or 10 min.
5. Wash 3 x 5 min with PBS.
6. Add 2 ml PBS and store at 4 ºC.

Table 2.15: PBS

Component	Final concentration	Quantity
KH_2PO_4	1.5 mM	0.24 g
KCl	2.7 mM	0.20 g
Na_2HPO_4	6.5 mM	1.44 g
NaCl	137.0 mM	8.01 g
Distilled water		ad 1000 ml

Adjust pH to 7.4 and autoclave.

2.5.2 Staining

Staining of the cells was performed as soon as possible after fixing. Two sets of antibodies were used: a primary antibody against the antigen of interest, and a secondary, fluorophore-coupled antibody, that recognized the primary antibody. The fluorescent dye 4', 6-diamidino-2-phenylindole (DAPI) was used to stain DNA in order to visualize cell nuclei.

Immunofluorescence procedure for CLSM imaging:

1. Remove PBS from culture dishes.
2. Add 50 µl pre-incubation solution (Table 2.16) for permeabilization and blocking onto parafilm.
3. Place one cover glass on the pre-incubation droplet (cells facing down).
4. Incubate at room temperature for 1 h.
5. Wash 3 times with PBS by dipping the cover glass into 3 beakers containing PBS.
6. Add 50 µl primary antibody solution (Table 2.16) onto parafilm.
7. Place the cover glass on the droplet.
8. Incubate at 4 ºC over night in a moist container.
9. Wash 3 times with PBS.
10. Add 50 µl secondary antibody solution (Table 2.16) onto parafilm.
11. Place the cover glass on the droplet.
12. Incubate in the dark at room temperature for 1 h.
13. Wash 3 times in PBS.
14. Add 50 µl DAPI working solution (Table 2.18) onto parafilm.
15. Place the cover glass on the droplet.
16. Incubate in the dark at room temperature for 10 min.
17. Wash once with PBS.
18. Mount 4 cover glasses on one object glass with 10 µl of FluorSave™ mounting medium for each cover glass.
19. Dry over night, seal with nail polish, and store in the dark.
20. Image in a CLSM.

Table 2.16: Immunofluorescence solutions

Component	Final concentration	Quantity
Pre-incubation solution		
5 % Triton X-100 (in PBS)	0.5 %	2.0 ml
Normal mouse serum	10 %	2.0 ml
PBS		16.0 ml
Make 4 ml aliquots. Store at -20ºC.		
Incubation solution		
5 % Triton X-100	0.5 %	2.0 ml
Normal mouse serum	3 %	600 µl
PBS		17.4 ml
Make 4 ml aliquots. Store at -20ºC.		
Primary antibody solution		
Dilute primary antibody 1:100 in incubation solution.		
Secondary antibody solution		
Centrifuge secondary antibody at 16 060 x g and 4 ºC, for 10 min.		
Dilute Cy™ 3 and Fluorescein isothiocyanat (FITC) 1:200 in incubation solution.		

Table 2.17: Antibodies

Primary antibodies
Nur-77 antibody (anti mouse nur-77 rabbit polyclonal IgG)
AIF antibody (anti mouse AIF goat polyclonal IgG)
Secondary antibodies
Cy™ 3-conjugated mouse anti-rabbit IgG
FITC -conjugated mouse anti-goat IgG

Table 2.18: Solutions for DAPI staining

Component	Quantity
DAPI stock (1 mg/ml)	
DAPI	1.0 mg
Physiological (0.9 % NaCl) saline	1.0 ml
DAPI working solution (10 000 x dilution)	
DAPI stock (1 mg/ml)	0.2 µl
5 % Triton X-100 stock	40.0 µl
PBS (Table 2.15)	2.0 ml

2.6 Graphing and Statistical Analysis

GraphPad Prism 4 software from GraphPad Software Inc., San Diego, USA, was used for graphing, while Sigma Stat 3.2 software from SPSS Inc., Chicago USA, was used for statistical analyses of data. An unpaired t-test was used for comparison of means of two groups. Multiple comparisons of means were analyzed by one way analysis of variance (ANOVA) and the Holm-Sidak method. If equal variance failed, multiple comparisons of medians were analyzed by Kruskal-Wallis one way ANOVA on ranks with Dunn's method. $P < 0.05$ was considered significant. Error bars of means in figures indicate standard error (SE).

3 Results

3.1 ATP-Depletion

3.1.1 Establishment of a Luminometric ATP Assay with Over-Expressed Luciferase in Cell Lysates for Validation of ATP-Depletions

To verify that cells used in FRAP experiments (section 3.2.1) were ATP-depleted, an assay for measuring ATP in a luminometer was established. CV-1 cells were transfected with the plasmid rsv-luc (section 2.1.2) to express the luciferase enzyme required in the luciferin oxidation reaction (section 1.5.3). The cells were harvested, and ATP from non-transfected cells or ATP-dilutions was measured in the luminometer (section 2.1.3). To correct for ATP present in the cells that expressed the luciferase enzyme, these cells were separately measured twice, and the mean value was subtracted as a negative control within every experiment. The values obtained could not be directly compared between all experiments because of varying concentrations of luciferase in cell lysates, and thereby differences in RLU measurements for the same amount of ATP.

Cell lysate from non-transfected cells, 50 µl, was measured with 10–40 µl of cell lysate from rsv-luc transfected cells to establish the lowest optimal amount of luciferase-containing cell lysate to be used. A small amount of rsv-luc containing cell lysate would reduce background ATP and substances that could affect the luciferin/luciferase reaction. The data are presented in Table 3.1.

Table 3.1: Luminometer measurements with varying volumes of cell lysate from cells transfected with rsv-luc.
Cell lysate from non-transfected cells (50 µl) was measured in the luminometer with cell lysate from luciferase-expressing cells to determine the minimum amount of luciferase containing cell lysate required for the ATP measurements (n=1).

Cell lysate from rsv-luctransfected cells (µl)	Signal (RLU)
40	703
20	422
10	234
5	60
0	65

The minimum amount of luciferase-containing cell lysate that provided a measurement above the background signal was 10 µl, and this amount was therefore used in the subsequent experiments.

To determine the linear range in the luminometer, a ten-fold dilution series of ATP, ranging from 2.4 mg/ml to 2.4 x10^{-5} mg/ml, was the initial measurement of every experiment. A dilution in the linear range would later be used as an internal standard in the ATP measurements. The data are presented in Figure 3.1.

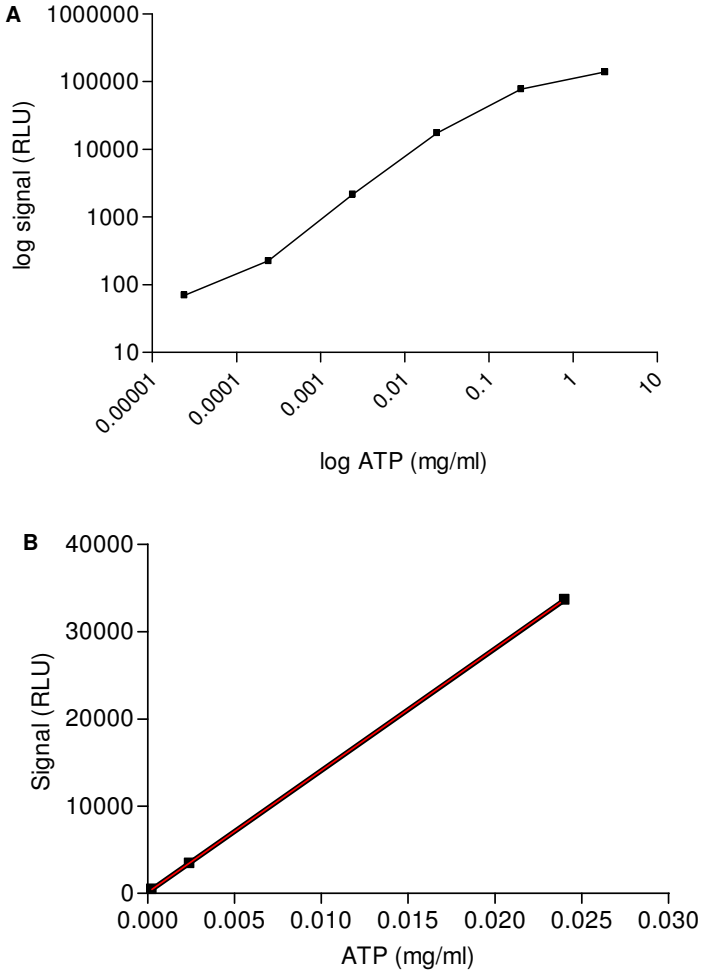

Figure 3.1: Luminometer measurements of a 10-fold dilution series of ATP.
Rsv-luc transfected cells were harvested to provide the luciferase enzyme required for measurements of ATP dilutions in the luminometer. The RLU-signal in samples with 10 µl from this cell extract and 50 µl of a 10-fold dilution series of ATP was measured. (A) The data were from 1 representative experiment out of 13 independent experiments and were subtracted the negative control value of 701 RLU. (B) Measurements of the 2.4 x10^{-2}/10^{-3}/10^{-4} mg/ml ATP dilutions were plotted to display the linearity in this range, with regression plotted in red (r^2=0.9999). The data were average from 3 representative experiments (RLR-values were comparable) out of 13 independent experiments.

RLU values from measurements of the 2.4 $x10^{-3}$ mg/ml ATP dilution were in the linear range. Consequently, this dilution was used as an internal standard in subsequent experiments to determine if there were substances present in the cell lysate that could affect the luciferin/luciferase reaction. Samples consisting of cell lysate from non-transfected cells (50 µl) and/or varying volumes of the 2.4 $x10^{-3}$ mg/ml ATP dilution were measured in the luminometer as displayed in Table 3.2. Cell lysate from rsv-luc transfected cells (10µl) was added to all samples to provide the luciferase enzyme. Loss of signal was calculated from the measurement of the 2.4 $x10^{-3}$ mg/ml ATP dilution by it self or multiplied by two to four, and added to the measurement of the cell lysate from non-transfected cells only.

Table 3.2: Luminometer measurements of varying volumes of the 2.4 $x10^{-3}$ mg/ml ATP dilution.
Cell lysate from non-transfected cells and/or varying volumes of the 2.4 $x10^{-3}$ mg/ml ATP dilution was measured in the luminometer with 10 µl of cell lysate containing the luciferase enzyme. Data were from 1 representative experiment out of 6 independent experiments and were subtracted the negative control of 610 RLU.

Cell lysate from non-transfected cells (µl)	ATP dilution (2.4 $x10^{-3}$ mg/ml) (µl)	Signal (RLU)	Loss of signal (%)
50	0	2305	
0	50	1633	
50	50	2591	35
50	100	2502	55
50	150	3328	56
50	200	3746	58

The results did not demonstrate an increase of signal corresponding to the amount of ATP added, thus indicating that the cell lysate was quenching the signal. The signal was reduced by 35-58 % from the predicted RLU values. In order to reduce the activity of ATPases or other factors that reduced the RLU signal, the non-transfected cells were harvested in solutions containing TCA before measurements. The effects on the quenching of the RLU-signal after harvesting the cells in boiling water or boiling of the cell lysate were also assayed. Cells expressing the luciferase enzyme were harvested according to the conventional protocol.

Non-transfected cells were harvested in TCA to precipitate proteins, as indicated in Table 3.3, and measured in the luminometer.

Table 3.3: Luminometer measurements of cell lysate from non-transfected cells harvested in varying concentrations of TCA.
Non-transfected cells were harvested in solutions containing TCA in order to precipitate proteins that could reduce the RLU signals. From the resulting cell lysate, 50 µl was measured with 10 µl of cell lysate from rsv-luc transfected cells that expressed the luciferase enzyme (n=1). The negative control (825 RLU) was not subtracted in the middle column, as this would result in negative RLU values. The negative control was subtracted in the right column, and negative RLU values were set to 0.

TCA (%)	Signal (RLU)	Signal (RLU) ÷ negative control
0	2551	1726
10.00	65	0
5.00	258	0
2.50	399	0
1.25	151	0

Cell harvesting with TCA lowered the RLU signals of non-transfected cell lysates to negative values after subtraction of the negative control. Hence, harvesting of cells with TCA was not a suitable method for reducing the activity of factors quenching the RLU signal. Boiling of the cell lysate from non-transfected cells could possibly reduce quenching as boiling MQ-H_2O would lysate cells and denature proteins. Non-transfected cells were harvested in boiling MQ-H_2O and measured alone, or with varying volumes of the 2.4 $x10^{-3}$ mg/ml ATP dilution, as specified in Table 3.4.

Table 3.4: Luminometer measurements of varying volumes of a 2.4 x10^{-3} mg/ml ATP dilution with cell lysate from non-transfected cells harvested in boiling water.
Non-transfected cells were harvested in boiling MQ-H_2O to denature proteins that possibly were quenching the RLU signal. The cell lysate was measured separately, or with an ATP-dilution. Luciferase was provided from 10 µl of cell lysate from rsv-luc transfected cells. The data were from 1 representative experiment out of 2 independent experiments.

Cell lysate from non-transfected cells (µl)	ATP Dilution with 2.4 x10^{-3} mg/ml (µl)	Signal (RLU)	Loss of signal (%)
50	0	1448	
0	50	720	
50	50	1496	31
50	100	1573	46

The results demonstrated a reduction of RLU signals if compared to the RLU value measured from the cell lysate from non-transfected cells by it self added to the value measured from the ATP-dilution by it self. However, the 31 % and 46 % loss of signals in this experiment represented a small improvement from the 35-58 % of signals that were lost in the measurements of cell lysates that were harvested without boiling water (Figure 3.2). This result indicated that the level of substances that quenched the RLU signal could to some extent be reduced by boiling. Consequently, boiling of the cell lysate after conventional harvesting in order to denature proteins and thereby inhibit quenching was also assayed. After boiling, the cell lysate was measured in the luminometer alone or with the 2.4 x10^{-3} mg/ml ATP dilution. The results are presented in Table 3.5.

Table 3.5: Luminometer measurements of varying volumes of a 2.4 x10^{-3} mg/ml ATP dilution with boiled cell lysate from non-transfected cells.
Non-transfected cells were harvested and boiled to denature proteins that could inhibit the luciferin/luciferase reaction. The cell lysate, and 10 µl of cell lysate containing luciferase, were measured alone or with an ATP dilution. Data were from 1 representative experiment out of 3 independent experiment, and were subtracted the negative control of 610 RLU.

Volume of cell lysate from non-transfected cells (µl)	Volume of the 2.4 x10^{-3} mg/ml ATP dilution (µl)	Signal (RLU)	Loss of signal (%)
50	0	2305	
0	50	1533	
50	50	2591	18
50	100	2502	6
50	150	3328	21
50	200	3746	22

Boiling of the cell lysate from non-transfected cells did not provide the increase in RLU values that could be predicted from the addition of ATP to the cell lysate from the non-transfected cells. However, the loss of signal was lower than in the measurements of cell lysates that were not boiled (Table 3.2). The reduction of RLU signals is displayed in Figure 3.2.

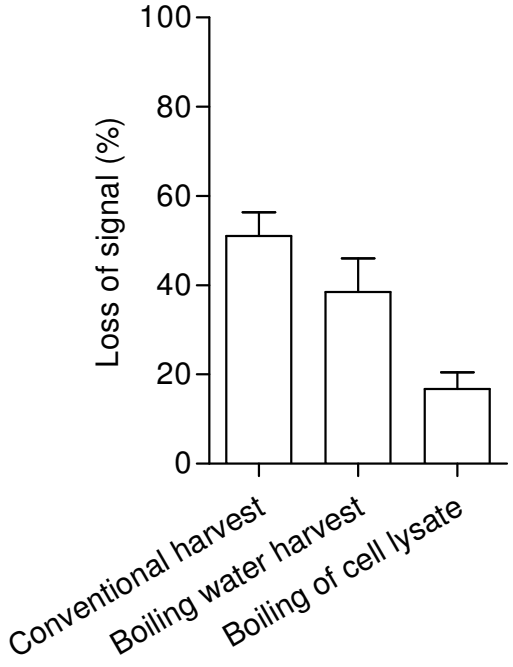

Figure 3.2: Loss of RLU signals in measurements of a 2.4 x10^{-3} mg/ml ATP dilution.
Different volumes of a 2.4 x10^{-3} mg/ml ATP dilution were added to cell lysates from a conventional harvest of non-transfected cells (Table 3.2) or lysates from non-transfected cells that were boiled during or after harvesting (Table 3.4 and Table 3.5). Reduction of predicted signal after adding of ATP was calculated in the given tables and is displayed as mean with SE.

Boiling of the cell lysate that was harvested from non-transfected cells reduced the loss of signal, thus, the method was used in subsequent experiments.

3.1.2 ATP-Depletion of CV-1 Cells

CV-1 cells were ATP-depleted by incubation for 2, 4, 6, and 16 hrs in a glucose–free cell medium supplemented with NaN_3 (section 2.1.3). Cells were harvested and cell lysates were boiled and measured in the luminometer (section 2.1.4). The results are displayed in Table 3.6.

Table 3.6: Luminometer measurements of cell lysate from ATP-depleted cells.
CV-1 cells were ATP-depleted in glucose-free medium supplemented with NaN_3. Cells were harvested and cell lysate was boiled and measured in a luminometer. Data were from 1 representative experiment out of 3 independent experiments.

Depletion time	Signal (RLU)	Percent of non-depleted
0 hrs	1620	100
2 hrs	1431	88
4 hrs	1362	84
6 hrs	204	13
16 hrs	27	2

The results showed a time-dependent decrease in ATP. Addition of internal standard in depleted cells showed a linear increase in RLU as in non-depleted cells (not shown), adding evidence to the linearity of the assay. Cells incubated for 16 hrs in glucose-free medium supplemented with NaN_3 had a 98 % loss of RLU signal. However, when culture dishes that contained these cells were viewed under a microscope, few or no cells were attached to the plastic. In contrast, the cells depleted for 6 hrs showed normal morphology and were still attached to the plastic. The 6 hrs of incubation was therefore used to obtain efficiently reduced ATP-levels in cells in subsequent experiments.

3.2 Nuclear Import of NGFI-B in CV-1 Cells

3.2.1 Energy Requirements for Transport of NGFI-B from the Cytoplasm into the Nucleus

The nuclear receptor NGFI-B contains two NLSs (Hsu *et al.*, 2004), and is consequently a candidate for energy dependent nuclear import pathways (section 1.2). The effect of ATP-depletion on nuclear import of NGFI-B was assayed in order to determine if the import was energy-dependent. CV-1 cells were transfected with GFP-tagged NGFI-B or GFP, and FRAP experiments were performed. The distribution of the fluorescent proteins in the CV-1-cells is displayed in Figure 3.3.

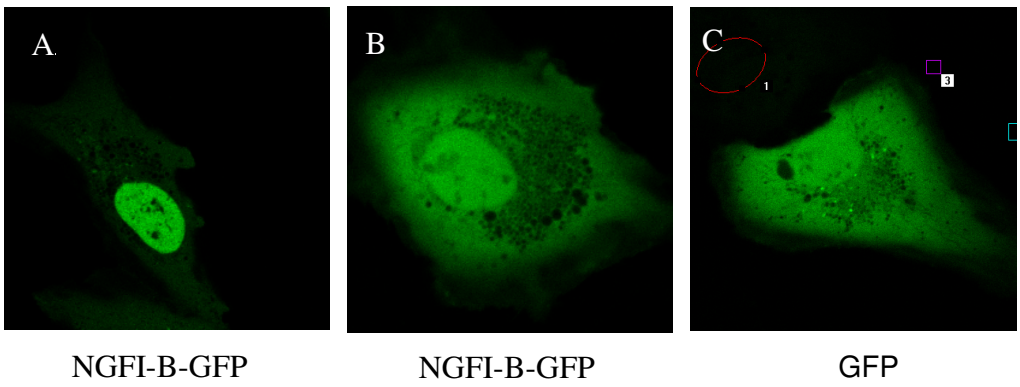

Figure 3.3: Cells transfected with NGFI-B-GFP or GFP alone.
CV-1 cells were transfected with NGFI-B-GFP or GFP to perform FRAP experiments. Cells were visualized in a CLSM. (A) The majority (80-90 %) of cells expressing NGFI-B-GFP had a higher concentration of fluorescent proteins in the nucleus than in the cytoplasm. (B) Some cells (10-20 %) had an even concentration of fluorescence in both cellular compartments, and these cells were selected for FRAP. (C) The concentration of GFP was evenly distributed between the nucleus and the cytoplasm.

The micrographs demonstrated a higher concentration of NGFI-B-GFP in the nucleus compared to the cytoplasm in the majority of CV-1 cells (80-90 %, data not shown), while the concentration of GFP was similar in both compartments. The NGFI-B-GFP-expressing cells that were visually selected for FRAP had a distribution of fluorescence that was similar to that of GFP (10-20 %, data not shown).

Nuclear FRAP (section 2.1.5) was measured by live cell imaging of CV-1 cells transfected with NGFI-B-GFP or GFP (section 2.1.2). GFP has a molecular weight of 27 kDa, and was expected to passively diffuse through the NPCs which usually only hinder molecules larger that 40 kDa. GFP was therefore used as a control for energy independent nuclear import in cells. FRAP was also performed on the nuclei of transfected CV-1 cells that were ATP-depleted in a glucose free medium supplemented with NaN_3 for 6 hrs (section 2.1.3). The initial slopes (0-22 s.) of the recoveries were calculated in order to quantify nuclear import and to minimize the impact of nuclear export. After photobleaching, the nuclear export was expected to play an increasing part in obtaining the equilibrium of fluorescence between the nucleus and the cytoplasm, as there would be increasingly more fluorescent molecules in the nucleus that could be exported. The results are presented in Figure 3.4.

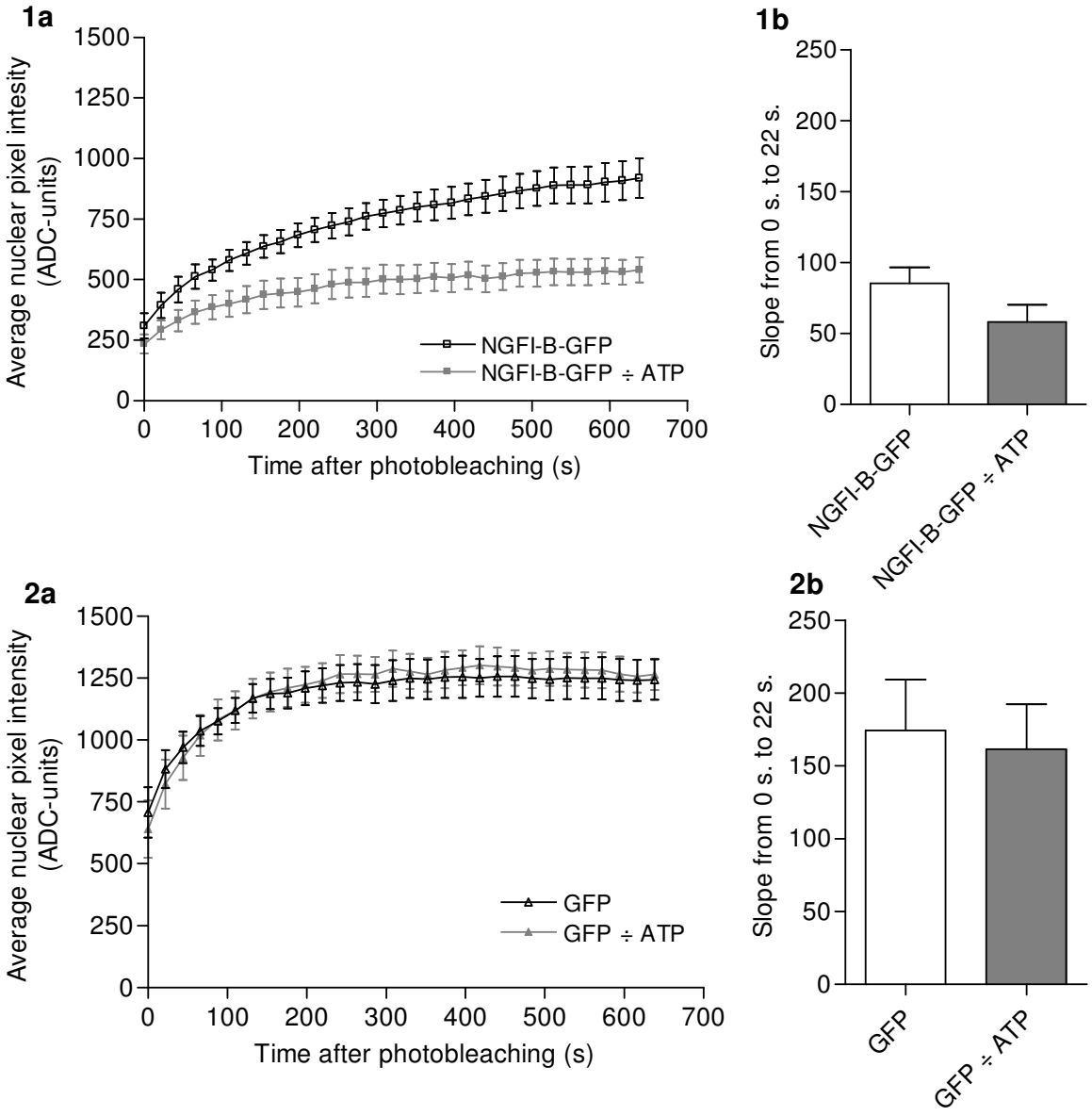

Figure 3.4: Nuclear fluorescence recovery after photobleaching of cells transfected with NGFI-B-GFP or GFP, with or without ATP-depletion.
CV-1 cells were transfected with NGFI-B-GFP (1) or GFP (2) and FRAP was performed on cell nuclei. FRAP was also performed after ATP-depletion of cells to investigate whether the nuclear import of NGFI-B was energy-dependent. Slopes from 0-22 s. were displayed as a measure of nuclear import (export contributed negligible) (b). Data from two independent experiments were displayed as mean with SE (n=9).

The results demonstrated a reduced import of NGFI-B-GFP (approximately 30 % reduction) in the nucleus of ATP-depleted cells, compared to non-depleted cells in the first 22 s. after bleaching. The nuclear import of GFP was approximately equal in the presence and absence of ATP (reduced by less than 10 %).

3.2.2 Effects of EGF or Phosphorylation of Threonine 142 on Nuclear Import of NGFI-B-GFP

Translocation of NGFI-B from the nucleus to mitochondria is demonstrated to induce apoptosis (Li *et al.*, 2000). The growth factor EGF activates ERK2 which phosphorylates Thr 142 in the amino terminal of NGFI-B (Slagsvold *et al.*, 2002), and is shown to reduce mitochondrial association of NGFI-B (Jacobs *et al.*, 2004). It was therefore interesting to investigate whether phosphorylation of Thr 142 in NGFI-B-GFP increased nuclear import of the nuclear receptor. The 142 threonine residue was mutated to alanine to block phosphorylation of this residue (NGFI-B-T142A-GFP), or to glutamate to mimic a constitutive phosphorylation (NGFI-B-T142E-GFP). CV-1 cells were transfected with NGFI-B-GFP, NGFI-B-T142A-GFP, or NGFI-B-T142E-GFP (section 2.1.2) and FRAP (section 2.1.5) was performed.

No changes of subcellular distribution of NGFI-B-GFP with or without Thr mutations were detected by a visual assessment (data not shown). The majority of the cells (80-90 %, data not shown) had a higher concentration of fluorescent proteins in the nucleus compared to the cytoplasm, while a minority (10-20 %, data not shown) of cells had a more similar concentration in both compartments (such as NGFI-B-GFP in Figure 3.3). Cells with a slightly more fluorescent nucleus than cytoplasm were visually selected for photobleaching. The nuclear fluorescence recovery after photobleaching was assayed and plotted in Figure 3.5. The results were presented as overall recovery and as the slope of the first 22 seconds after photobleaching. The initial slopes of the recoveries were calculated in order to quantify nuclear import and to minimize the impact of nuclear export (section 3.2.1).

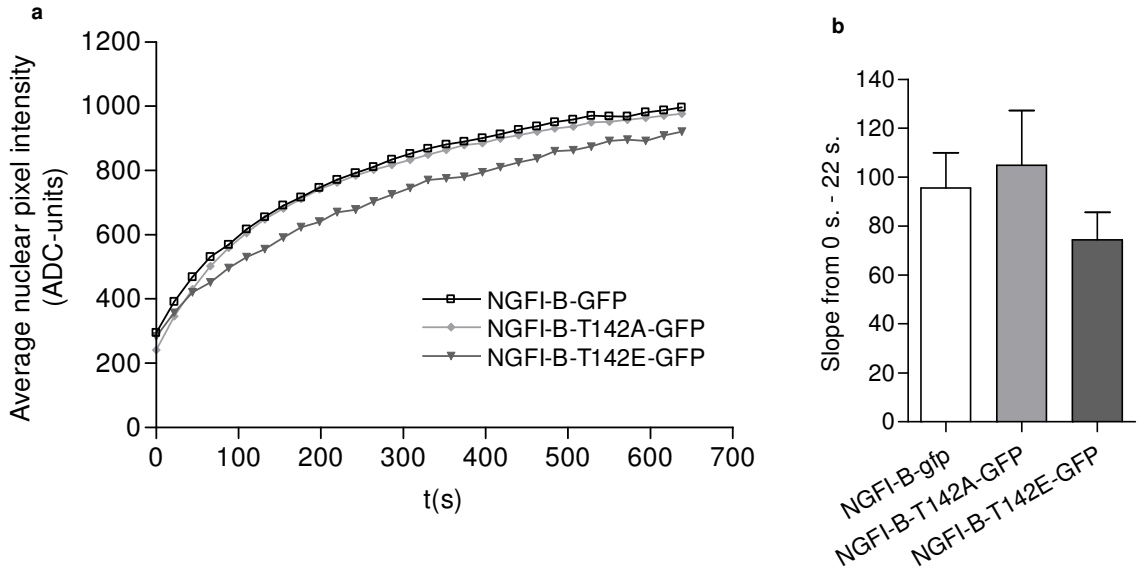

Figure 3.5: Recovery of nuclear fluorescence after photobleaching in cells transfected with NGFI-B-GFP, NGFI-B-T142A-GFP, and NGFI-B-T142E-GFP.
CV-1 cells were transfected with NGFI-B-GFP, NGFI-B-T142A-GFP (to block phosphorylation), and NGFI-B-T142E-GFP (to mimic the phosphorylated state of Thr 142). The effect of the mutations on nuclear import of NGFI-B was investigated by nuclear FRAP. The slopes from 0-22 s after photobleaching were displayed as a measure of nuclear import. Data from two independent experiments were plotted as mean (a) or displayed as mean with SE (b) (n=8 or 9).

The results demonstrated that a 142 threonine-to-alanine mutation that blocked phosphorylation of this residue slightly increased the nuclear import of NGFI-B-GFP after photobleaching (~10 % increase). The nuclear import of NGFI-B with a 142 threonine that was mutated to glutamate to mimic phosphorylation was reduced by approximately 25 %.

To determine the steady state distribution of NGFI-B, NGFI-B-T142A-GFP, and NGFI-B-T142E-GFP before FRAP, the ratios of nuclear fluorescence to fluorescence in the cytoplasm were calculated. The results are displayed in Figure 3.6.

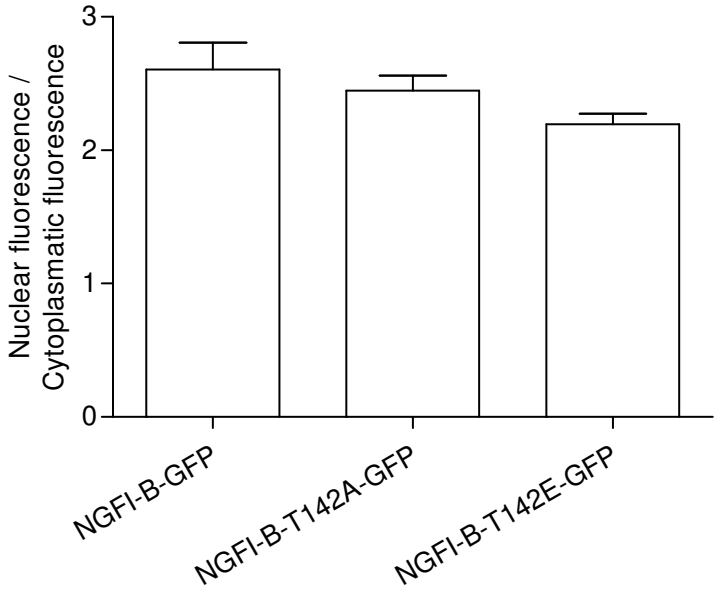

Figure 3.6: Pre-bleach ratio of nuclear to cytoplasmic fluorescence.
CV-1 cells were transfected with NGFI-B-GFP, NGFI-B-T142A-GFP (to block phosphorylation), and NGFI-B-T142E-GFP (to mimic phosphorylation of Thr 142). The effects of these mutations on the ratio of nuclear to cytoplasmic fluorescence were calculated. The data from two independent experiments were displayed as mean with SE (n=8-9).

Cells transfected with NGFI-B-GFP displayed the highest ratio of nuclear to cytoplasmic fluorescence while cells transfected with NGFI-B-T142E-GFP had the lowest.

The results in Figure 3.5 and Figure 3.6 demonstrated an opposite effect of what was hypothesized. FRAP was therefore performed on CV-1 cells transfected with NGFI-B-GFP and treated with EGF, in order to determine whether EGF promoted nuclear import of NGFI-B in these cells. The results are presented in Figure 3.7.

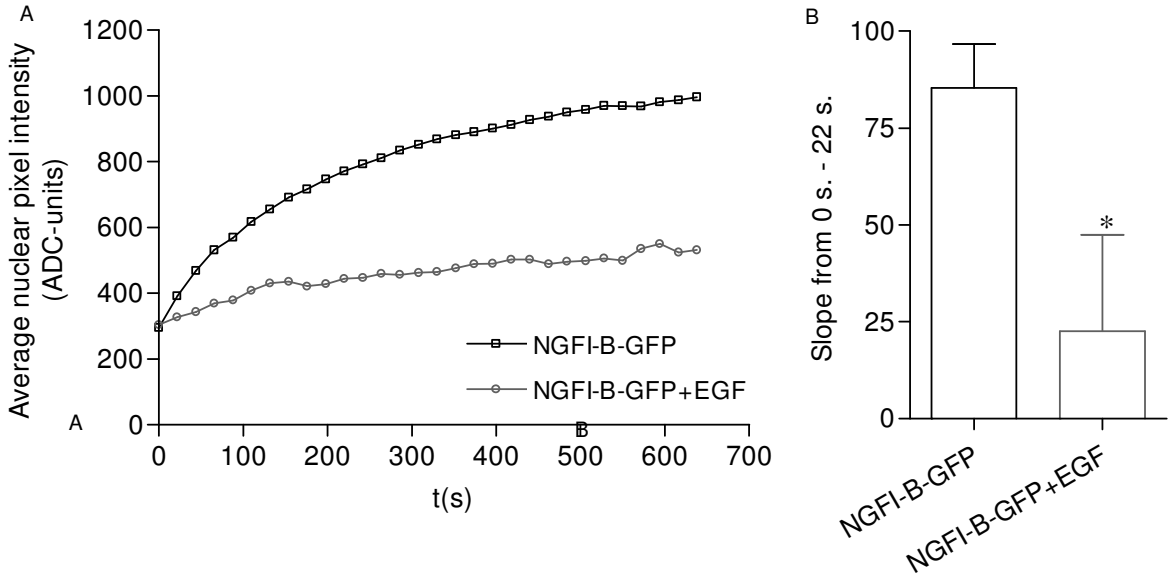

Figure 3.7: Nuclear recovery of fluorescence after photobleaching in cells that were transfected with NGFI-B-GFP and treated with EGF.
CV-1 cells were transfected with NGFI-B-GFP, and treated with EGF (5 ng/ml) 10 min prior to nuclear FRAP. The slope from 0-22 s. was calculated. The data from 1 to 2 independent experiments were plotted as mean (A), or displayed as mean with SE (B) (n=4 or 9). *P < 0.05 compared with NGFI-B-GFP (unpaired t-test).

The pre-bleach ratio of nuclear to cytoplasmic fluorescence was approximately equal with or without EGF treatment (data not shown).The results demonstrated that cells treated with EGF for 10 min prior to nuclear photobleaching had a significantly decreased (~75 %) nuclear import of NGFI-B-GFP.

3.3 Effects of Dominant Active or Dominant Negative ERK2 on Nuclear Import of NGFI-B

ERK2 phosphorylates Thr 142 in the amino terminal of NGFI-B (Slagsvold *et al.*, 2002) and is shown to diminish the concentration of NGFI-B in the cytoplasm (Jacobs *et al.*, 2004). However, the results in section 3.2.2 demonstrated that the mutation mimicking phosphorylation of Thr 142 in NGFI-B reduced the nuclear import of NGFI-B. It was therefore interesting to investigate whether a dominant active or negative ERK2 would increase or decrease nuclear import of NGFI-B-GFP.

NGFI-B was co-transfected with dominant active or negative ERK2 in CV-1 cells (section 2.1.2), and nuclear FRAP was performed (section 2.1.5). Slopes from 0 s–22 s were calculated to quantify nuclear import. The results are presented in Figure 3.8.

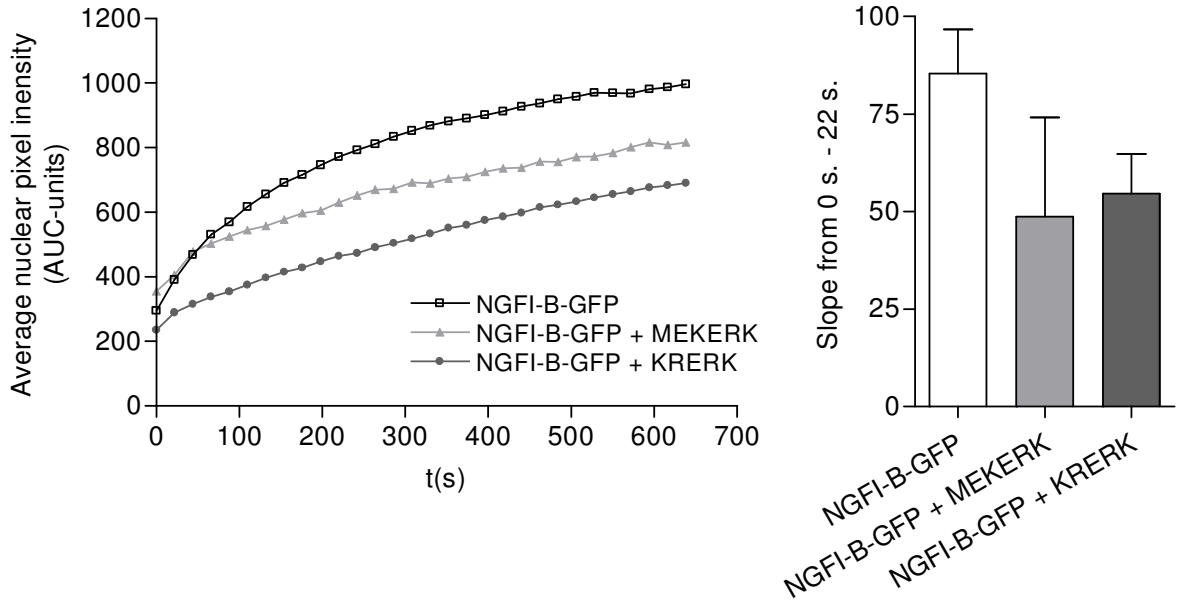

Figure 3.8: Nuclear recovery of fluorescence after photobleaching in cells co-transfected with NGFI-B-GFP, and dominant active or negative ERK2.
Nuclear FRAP was performed in CV-1 cells that were co-transfected with NGFI-B-GFP and dominant active ERK2 (MEKERK2) or dominant negative ERK2 (KRERK2). The slopes from 0-22 s were calculated. Data from 2 independent experiments were plotted as mean or displayed as mean with standard error (SE) (n=4 -10).

The pre-bleach ratios of nuclear to cytoplasmic fluorescence were approximately equal between NGFI-B-GFP and NGFI-B-GFP co-transfected with dominant negative or active ERK2 (data not shown). The nuclear import of NGFI-B-GFP after photobleaching was reduced in cells over-expressing dominant active ERK2 (~45 % reduction) or dominant negative ERK2 (~35 % reduction).

3.4 Cerebellar Granule Neurons

3.4.1 Glutamate-Induced Cell Death of CGN

NGFI-B is highly expressed in neurons and is shown to translocate to mitochondria in glutamate-exposed CGN. This translocation is inhibited by EGF, which is shown to activate ERK2 of the

MEK/ERK cascade in CGN (Jacobs *et al.*, 2004). Retention of NGFI-B in the nucleus could protect cells from glutamate damage. However, ERK activation is also a consequence of glutamate exposure, in which the ERK activation contributes to cell death (Zhou *et al.*, 2007). The effect of EGF stimulation of cells before glutamate exposure was assayed. The effect of MEK inhibitor U0126 on glutamate-induced death of CGN when added before or after glutamate exposure was also investigated, and dying cells were stained by trypan blue (section 2.4). In primary cultures, cell death may vary between the preparations, and experiments that induced ~100 % cell death were disregarded because necrosis was likely to have contributed. The cell death counts are displayed in Figure 3.9.

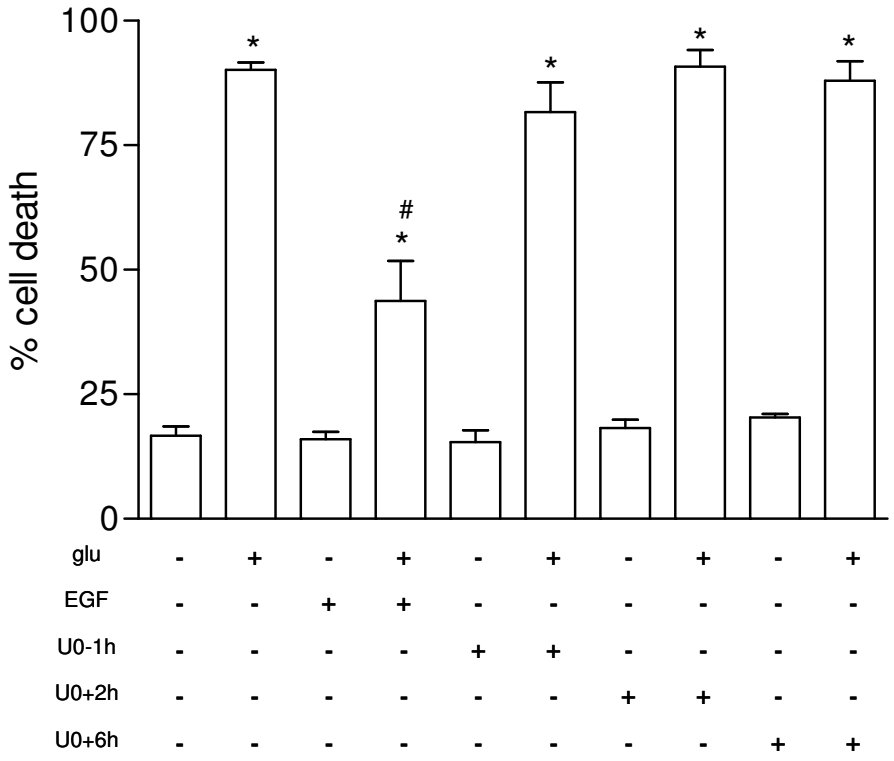

Figure 3.9: Effect of MEK inhibitor U0126 and EGF on glutamate-induced cell death.
CGN were incubated with MEK inhibitor U0126 1 h before (U0-1h), or 2 or 6 hrs after (U0+2h/6h) glutamate exposure to assay the effects on cell death. CGN were also pre-incubated with EGF (5 ng/ml) for 15 min prior to glutamate exposure, or just exposed to glutamate (glu). The results were displayed as mean with SE of cell death counts in percent of total cells (n=5-14). Data were from 5 independent experiments. $^{*}P < 0.05$ compared to respective controls that were not exposed to glutamate (one way ANOVA with the Holm-Sidak method). $^{\#}P < 0.05$ compared to glutamate exposure alone (Kruskal-Wallis one way ANOVA on ranks with Dunn's method (equal variance failed).

All treatments with glutamate resulted in significantly higher cell death than the control exposures. The glutamate-induced cell death was significantly reduced by pre-incubation with EGF. Cell death induced by glutamate was not prevented by post-incubation with MEK inhibitor U0126. However, pre-incubation with U0126 slightly reduced the death of glutamate-exposed cells compared to cells exposed to buffer, in four out of five independent experiments. The buffer-exposed cells showed a reduced death by pre-incubation with U0126 in two out of five experiments if compared to cells only exposed to buffer.

3.4.2 Subcellular Localization of NGFI-B and Apoptosis Inducing Factor in CGN

The subcellular localization of NGFI-B in CGN was investigated in order to establish whether this *in vitro* model was suited for further studies of neuronal traffic of NGFI-B. AIF promotes apoptosis by translocation from mitochondria to the nucleus (Susin *et al.*, 1999), and the subcellular localization AIF was therefore investigated as a marker of apoptotic mitochondrial activation. Rat CGN were exposed to physiological buffer or glutamate and double-immunostained to visualize NGFI-B and AIF, while cell nuclei were stained with DAPI. The CGN were examined in a CLSM, and micrographs were displayed in Figure 3.10 and Figure 3.11.

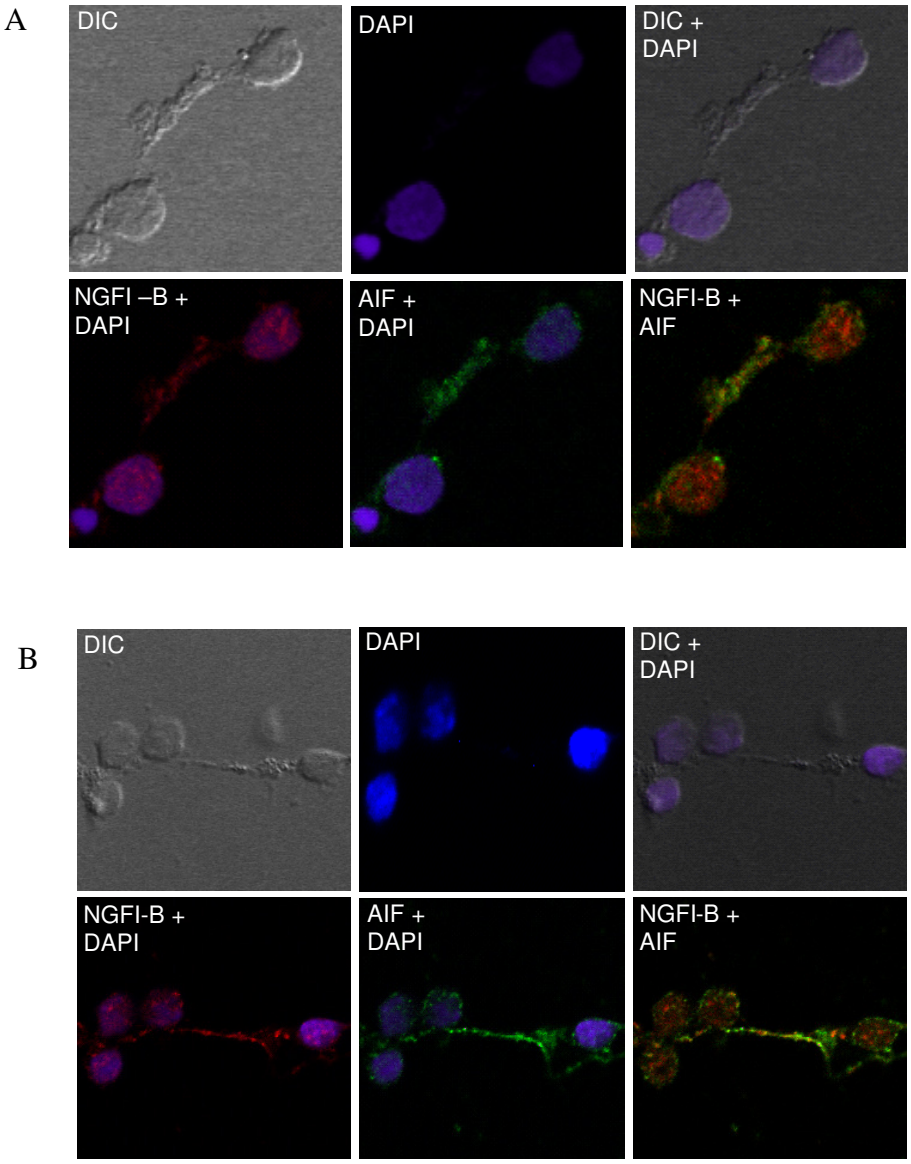

Figure 3.10: Micrographs of CGN that were exposed to glutamate or physiological buffer. Cells were DAPI- and immunostained.
CGN were exposed to physiological buffer (A) or glutamate (B), fixed, and NGFI-B and AIF were immunostained to determine their subcellular localizations. Cell nuclei were stained by DAPI. The top left image depicts cells using differential interference contrast (DIC). The image in the middle of the top row shows DAPI-stained cells, while the top right image is an overlay of DIC and DAPI staining. The left image on the bottom row is an overlay of NGFI-B stained with CY-3 and DAPI, and in the lower middle image is FITZ-stained AIF overlaid with DAPI. The image to the bottom right is an overlay of immunostained NGFI-B and AIF.

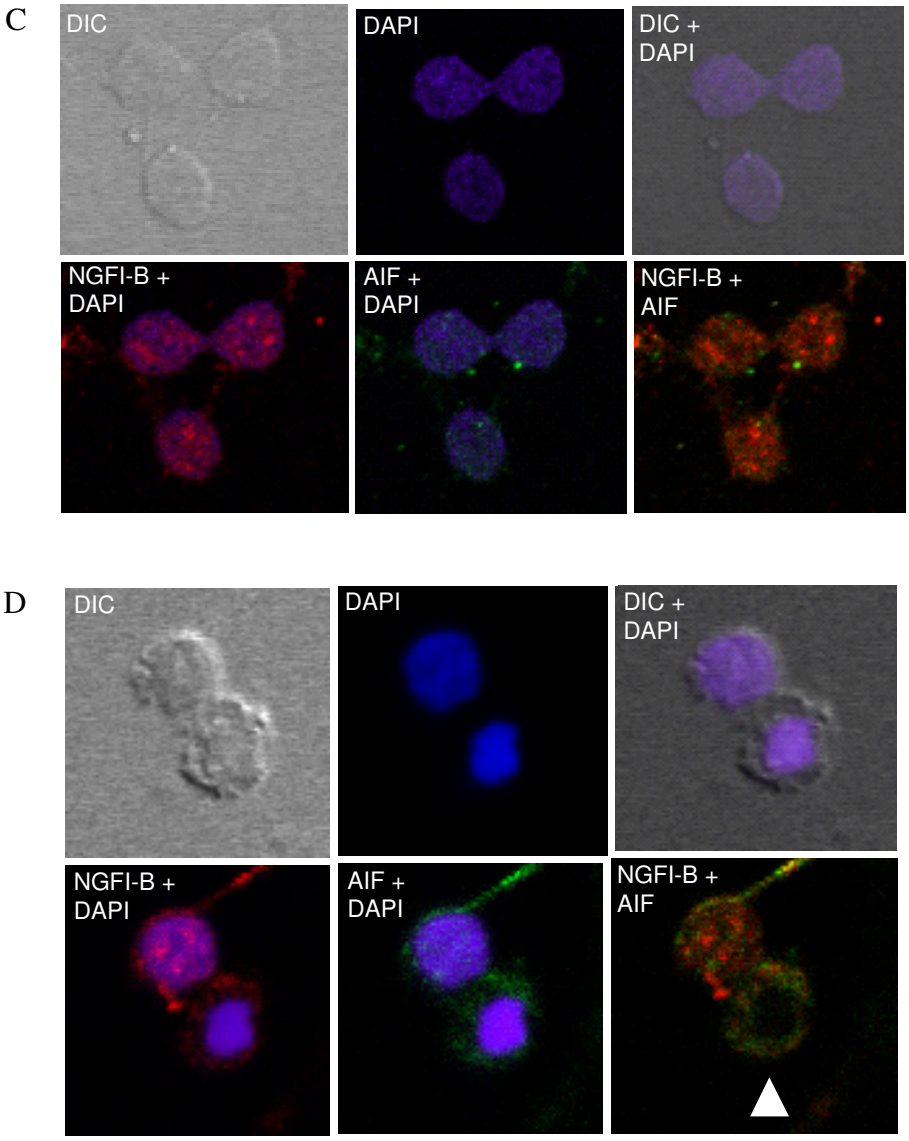

Figure 3.11: Micrographs or CGN that were exposed to glutamate. Cells were DAPI- and immunostained.
CGN were exposed to glutamate, fixed, and NGFI-B and AIF were immunostained to determine their subcellular localizations. Cell nuclei were stained by DAPI. The top left image of A and B shows cells using DIC. The image in the middle of the top row shows DAPI-stained cells, while the top right image is an overlay of DIC and DAPI staining. The left image on the bottom row is an overlay of NGFI-B stained with CY-3, and DAPI, and in the lower middle image is FITZ stained AIF overlaid with DAPI. The image to the bottom right is an overlay of immunostained NGFI-B and AIF.

In the majority of glutamate-exposed CGN, NGFI-B was distributed in the nucleus and in the cytoplasm, while AIF mainly was localized in the cytoplasm (B). This distribution was similar to that of CGN exposed to physiological buffer (A). The CLSM imaging revealed a small minority of glutamate-exposed CGN that showed a strongly reduced staining of AIF (C). Such cells had NGFI-B localized to both the cytoplasm and the nucleus. In a small fraction of the glutamate-exposed cells, NGFI-B was not situated in the nucleus, only in the cytoplasm, and AIF displayed a similar distribution as NGFI-B in such cells (indicated by an arrow in D).

4 Discussion

The orphan nuclear receptor NGFI-B (section 1.1) promotes the expression of survival molecules when acting as a transcription factor in the nucleus (Moll *et al.*, 2006). However, in response to apoptotic stimuli, NGFI-B may translocate to mitochondria and trigger apoptosis (section 1.4.3) (Lin *et al.*, 2004). This unique property of NGFI-B makes it a possible target for cancer therapeutics that promote apoptosis, and for pharmaceuticals that prevent neuronal apoptosis in neurodegenerative disorders. Many questions regarding the translocation of NGFI-B remain to be solved. This thesis will investigate several aspects regarding the regulation of NGFI-B migration.

4.1 Establishment of a Luminometric ATP-assay with Over-Expressed Luciferase in Cell Lysates for Validation of ATP-Depletions

4.1.1 Luminometric ATP-assay in CV-1 Cells

An ATP-measuring assay was developed to verify that cells used in FRAP experiments (section 4.3) were ATP-depleted. ATP is often determined by using a luciferin/luciferase reaction system (section 1.5.3) (Yang *et al.*, 2002) where the production of bioluminescence is measured in a luminometer. The luciferase enzyme was produced by the transfection of rsv-luc plasmids into cells that later would over-express the enzyme. The luciferase enzyme was extracted by harvesting of the rsv-luc transfected cells, and could then be used to determine if ATP levels in cell lysates from ATP-depleted cells were decreased (section 4.2).

The amount of luciferase-containing cell lysate that would be used to measure ATP was kept at a minimum to reduce background ATP and the presence of substances that could affect the luciferin/luciferase system. The results (Table 3.1) demonstrated that 10µl of cell lysate was the smallest measured amount that resulted in adequate ATP measurements.

To establish the linear range in the luminometer, a dilution series of ATP was measured in every experiment. Measurements of the 2.4 $x10^{-3}$ mg/ml ATP dilution were in the linear range (Figure 3.1), and a 10-fold increase of the amount of added ATP yielded a 10-fold increase of signal. Consequently, subsequent measurements were going be in this range, and the 2.4 $x10^{-3}$ mg/ml

ATP dilution would therefore be used as an internal standard. Measurements of the dilutions in separate experiments displayed great variations in RLU signals, strongly indicating that the concentration of luciferase varied in the cell lysates. Such variations could be a result of different transfection efficiencies or cell densities, and the comparison of absolute values between experiments was impractical in most experiments. It also became evident that measured values from one sample would slightly differ if measured several times. However, values were not obtained from multiple measurements of one sample because it was prioritized to measure all samples as quickly as possible to avoid decay of the luciferase enzyme or ATP. An exception was made with the negative control values that were the first and last measured sample from each round of cell harvest.

To determine if substances present in the cell lysate could inhibit or augment the luciferin/luciferase reaction, the internal ATP standard was added to the cell lysate of non-transfected cells and measured. The results (Table 3.2) did not display the increase of signal that would correlate to the increase of added ATP. The 10-fold increase of signal from the 10-fold increase of added ATP in the preceding measurement (Figure 3.1 B) displayed such a correlation. Accordingly, there were substances in the cell lysate that quenched the signal, such as ATPases or other energy consuming enzymes that depleted ATP, and/or substances that otherwise interfered with the luciferin/luciferase reaction. To address these issues, cells were either harvested in TCA that would precipitate proteins, or in boiling water that would denature proteins that quenched the RLU signal. In addition, cell lysate from cells harvested according to the original protocol was boiled.

Cells were harvested in solutions containing TCA as a modification of an existing ATP measurement procedure used by Berg-Johansen *et al.* (1993). When non-transfected cells were harvested in TCA, the RLU signal was reduced to zero (Table 3.3). This indicated that not only ATP-depleting enzymes, but also the luciferase enzyme, was precipitated to such an extent that there was not enough enzyme left to catalyze the luciferin oxidation reaction. Consequently, cells were not harvested in solutions containing TCA in subsequent experiments. A method developed by Yang *et al.* (2002), in which cells were harvested in boiling MQ-H_2O, was reported to inhibit ATPases and not to interfere with the bioluminescence. This method, in addition to boiling of

conventionally harvested cell lysates, was assayed. The boiling methods still resulted in quenching of the RLU values (Table 3.4 and Table 3.5). However, the loss of signal was reduced by approximately 70 % when the cell lysate was boiled after harvest, if compared to cell lysate that was not boiled (Figure 3.2). This indicates that the substances that quenched the RLU signal were eliminated to some extent. Quenching was similar at all ATP concentrations measured, and the method could therefore be used to determine percent ATP depletion in subsequent experiments (section 4.2 and 4.3).

4.2 ATP-Depletion of CV-1 Cells

ATP-depleted and non-depleted CV-1 cells were later going to be used in FRAP experiments to determine if nuclear import of NGFI-B was energy-dependent (section 3.2.1). The CV-1 cells were ATP-depleted in a glucose-free medium that was supplemented with sodium azide according to a procedure by Goda *et al.* (2002). Cells depleted for various time periods were harvested and measured to determine the required duration of the ATP-depletion procedure.

The results demonstrated that ATP-depletion for six hours strongly reduced RLU signals compared to signals from non-depleted cells, while shorter ATP-depletion resulted in a small reduction of signal. The ATP-depletion of CV-1 cells by sodium azide was slow compared to the ATP-depletion for 30 minutes in human epidermoid carcinoma cells and mouse fibroblasts by Goda *et al.* (2002). However, the cells that were depleted over night were no longer attached to the plastic surface of the culture dish. This strongly indicates that the cells were injured or dead. The cells that were depleted for six hours had a normal morphology and were attached to the culture dish, and this duration of ATP depletion was therefore used in FRAP experiments (section 4.3).

4.3 FRAP Experiments to Determine if Nuclear Import of NGFI-B is Energy-Dependent

The nuclear receptor NGFI-B has a molecular weight of 61 kDa (Fahrner *et al.*, 1990), and is therefore too large to passively diffuse through nuclear pores. However, NGFI-B contains two

NLSs (Hsu *et al.*, 2004) and is consequently a candidate for energy-consuming nuclear import pathways (section 1.2). To determine if nuclear import of NGFI-B is energy-dependent, NGFI-B-GFP was over-expressed in CV-1 cells, and FRAP experiments were performed before and after ATP-depletion of cells. The molecular weight of GFP is 27 kDa and it would therefore be small enough to passively diffuse through NPC. Furthermore, a similar concentration of GFP in both the nucleus and the cytoplasm (Figure 3.3) was suggested by Xiao *et al.* (2000) to indicate the absence of a NLS in GFP. Consequently, GFP was used as a control protein.

Cells with a slightly more fluorescent nucleus than cytoplasm after transfection with NGFI-B-GFP were visually selected for photobleaching (10-20 % of cells, data not shown). This made it possible to identify the nuclei, and at the same time have enough visible fluorescent molecules in the cytoplasm to obtain a recovery of fluorescence in the bleached nuclei (Figure 3.3). Such a distribution also resembled the subcellular localization of the over-expressed control protein, GFP.

The results demonstrated that nuclear import of NGFI-B was reduced by ATP-depletion (Figure 3.4). The depletion of ATP would also have diminished other nucleoside triphosphates generated by phosphate transfer from ATP to nucleoside diphosphates catalyzed by diphosphate kinases (Mourad and Parks, 1965). Consequently, the Ran GTPases that provided energy for nuclear import pathways would be depleted as well. It was demonstrated by Schwoebel *et al.* (2002) that ATP-depletion inhibited Ran-dependent nuclear import, and that such inhibition resulted from a shortage of RanGTP rather than the inhibition of some ATP-dependent process. The reduction of nuclear import of NGFI-B in ATP-depleted CV-1 cells therefore indicates that nuclear import of NGFI-B is energy-dependent. Alternatively, the nuclear import of NGFI-B could have been reduced by cell injuries as a consequence of the ATP-depletion. ATP-depletion is known to cause a series of cellular injuries that possibly could have affected the nuclear import of NGFI-B, including elevated intracellular calcium, loss of membrane-cytoskeleton linkage, and alteration of the function and/or aggregation of membrane proteins (Chen *et al.*, 1997; Chen *et al.*, 1994; Chen and Wagner, 2001; Haggie *et al.*, 2002; Wheeler *et al.*, 2000). However, visual differences in the microscope between cells that were ATP-depleted and the non-depleted cells were not detected (data not shown). This indicated that the cells were not severely damaged.

To optimize the FRAP assay, it would be recommended in future experiments to use another control protein than GFP. This protein should be the same size as NGFI-B, but without any sequences that could affect nuclear import or export, and it should be fused to GFP. NGFI-B has the molecular weight of 60 kDa, and the adding of GFP to NGFI-B made the molecule 87 kDa. The increase in size could possibly have affected the nuclear import of NGFI-B. In future experiments, this issue could be avoided by removing a 27 kDa part from NGFI-B. However, it would be crucial that the removed section does not contain features that are essential for the import pathways recognition of cargo, or that it affects other features of the nuclear import.

4.4 Nuclear FRAP of CV-1 cells Over-Expressing Threonine to Alanine or Glutamate Mutated NGFI-B

The subcellular localization of NGFI-B is reported to be regulated by phosphorylations of multiple serine and threonine sites (Han *et al.*, 2006; Kang *et al.*, 2000; Li *et al.*, 2000; Slagsvold *et al.*, 2002). Heavily phosphorylated NGFI-B is predominant in the cytoplasm while less phosphorylated NGFI-B localizes to the nucleus (Fahrner *et al.*, 1990). Jacobs *et al.* (2004) have previously demonstrated that the growth factor EGF activated the MAP kinase ERK2, and inhibited apoptosis-induced translocation of NGFI-B from the nucleus to the mitochondria. As EGF stimulation is shown to lead to phosphorylation of NGFI-B in PC12 cells (Hazel *et al.*, 1991), and since the threonine 142 of NGFI-B is phosphorylated *in vitro* ERK2 (Slagsvold *et al.*, 2002), the Thr 142 phosphorylation could be involved in the accumulation of NGFI-B in the nucleus. Nuclear import of NGFI-B was demonstrated to be energy-dependent in this thesis (section 4.3) and the presence of NLSs and NESs in NGFI-B makes it a potential cargo for classical nuclear import/export pathways. It was therefore interesting to examine whether phosphorylation of Thr 142 increased the rate of nuclear import of NGFI-B, and if elimination of phosphorylation of this site decreased this import.

CV-1 cells were transfected with NGFI-B-GFP, NGFI-B-GFP with a threonine 142 to alanine mutation (NGFI-B-T142A-GFP) that blocked phosphorylation of this residue, and NGFI-B-GFP with a threonine to glutamate mutation (NGFI-B-T142E-GFP) that functionally mimicked the

charge conferred by the phosphate. Nuclear recovery of the fluorescent proteins after photobleaching of the nuclei was assayed to investigate differences in nuclear import.

Surprisingly, the nuclear recovery of NGFI-B-GFP was slightly increased by blocking phosphorylation of Thr 142 (Figure 3.5). However, the similar recovery of NGFI-B-GFP and NGFI-B-T142A-GFP suggests that NGFI-B-GFP was basally non-phosphorylated at this residue. NGFI-B with a 142 Thr to Glu mutation that mimicked phosphorylation displayed a reduced recovery in the nucleus after photobleaching (Figure 3.5). These results indicate that the glutamate mutation affected NGFI-B as cargo for nuclear import pathways in such a manner that nuclear import was decreased.

Differences between the pre-bleach subcellular distribution of NGFI-B-GFP, NGFI-B-T142A-GFP, or NGFI-B-T142E-GFP were not visually detected. In a majority of CV-1 cells (80-90 %, data not shown), the concentration of fluorescent protein was higher in the nucleus than in the cytoplasm. However, a further increase of nuclear fluorescence would have been difficult to visually detect. If one of the fluorescent proteins demonstrated an increased import and localization to the nucleus, it would possibly have a decreased concentration in the cytoplasm. During bleaching of the nucleus, the remaining cytoplasmic proteins would have a rapid import in to the nucleus, where they would have been bleached. The amount of cytoplasmic fluorescent protein would thereby have been further reduced. Nuclear FRAP performed on such a cell would result in a slow recovery of nuclear fluorescence in despite of the high nuclear import rate. To address these issues, the ratio of nuclear to cytoplasmic fluorescence before bleaching was calculated (Figure 3.6). The exact values of nuclear fluorescence could not be used because the gain was changed within experiments, and thereby, the pixel intensity was also changed. A constant gain could not be sustained, as this reduced the visibility of a number of cells that was required to outline the nucleus for bleaching, and saturated others. The results demonstrated that NGFI-B-GFP had the highest fraction of total fluorescence in the nucleus, while that of BT142A-GFP was slightly lower. NGFI-B-T142E-GFP had the lowest nuclear to cytoplasmic ratio. These results confirmed a reduced nuclear import of NGFI-B-GFP with a Thr 142 Glu mutation that mimicked phosphorylation, and that this was not an effect of reduced cytoplasmic fluorescence.

Experiments by Slagsvold *et al.*(2002) demonstrated that EGF activated ERK2, and that ERK2 phosphorylated Thr 142 of NGFI-B. Furthermore, NGFI-B-GFP treated with EGF was documented to localize to the nuclei of CV-1 cells in a paper by Jacobs *et al.* 2004. However, in the experiments presented in the current thesis, translocation of NGFI-B-GFP into the nucleus may not be due to phosphorylation of Thr 142 by ERK2, as the nuclear import of NGFI-B was reduced by mimicking of this phosphorylation. Surprisingly, results also demonstrated that EGF-treatment of CV-1 cells resulted in a significantly reduced nuclear import of NGFI-B (Figure 3.7). It is tempting to speculate that EGF activated ERK2, which in turn phosphorylated Thr 142 of NGFI-B-GFP and thereby reduced nuclear import. In addition to phosphorylation of NGFI-B, ERK2 could have phosphorylated proteins involved in the regulation of nuclear import (Poon and Jans, 2005). Interestingly, several NPC proteins (nucleoporins, Nups) are themselves modified via phosphorylation by kinases that are involved in phosphorylation of NGFI-B (Eblen *et al.*, 2003; Frosst *et al.*, 2002).

EGF and phosphorylation of NGFI-B-GFP Thr 142 does not seem to have the same effects in experiments performed in this thesis and by Jacobs *et al.* (2004). The experiments were performed in the same laboratory and within the same CV-1 cell line. However, the serum batch used in the culture media was changed, in addition to thawing of new cells. These factors could have contributed to the observed alterations by a different composition of mitogens or other substances in serum, or an alteration within the cells themselves. NGFI-B-GFP in the present thesis had a higher concentration in the nucleus of the majority of CV-1 cells (Figure 3.3), while it was evenly distributed in the results presented by Jacobs *et al* (2004). This suggests that a change in the cell line has taken place. The subcellular distribution of NGFI-B is known to differ between cell lines (Fahrner *et al.*, 1990). Interestingly, the effect of EGF is also known do diverge; it is known to be a potent growth factor (Jorissen *et al.*, 2003), while in some tumor cell lines, EGF stimulation results in apoptosis (Chen *et al.*, 2004; Kottke *et al.*, 1999; Zhao *et al.*, 2006). Accordingly, there are a number of factors that could have contributed to the different results demonstrated by Jacobs *et.al.* (2004) and the present thesis. Additional experiments in order to reveal the cause of the alteration may further enlighten the mechanisms of the MEK/ERK pathway and translocation of NGFI-B.

In summary, by mimicking a phosphorylation of Thr 142 of NGFI-B-GFP, the nuclear import of the nuclear receptor was reduced compared to non-mutated NGFI-B. By blocking this phosphorylation, the nuclear import of NGFI-B-GFP was slightly increased. One of the most common mechanisms for down- regulating the efficiency of nuclear import is masking of NLSs within cargo proteins to prevent recognition by importins. The NLS can be masked by altered charge or conformational change due to phosphorylations (Poon and Jans, 2005). It is tempting to speculate that phosphorylation of Thr 142 in the N-terminal of NGFI-B masked one of the NLSs located in the C-terminus.

4.5 Nuclear FRAP in CV-1 cells over-expressing NGFI-B and Dominant Active or Negative ERK2

The MAP kinase ERK2 was demonstrated to phosphorylate Thr 142 in the amino terminal of the nuclear receptor NGFI-B (Slagsvold *et al.*, 2002). In studies by Jacobs *et al.* (2004) and Jacobs and Paulsen (2005), NGFI-B-GFP expressed in the presence of dominant active ERK2 localized to the nucleus of CV-1 cells. These results suggested that phosphorylation of Thr 142 by ERK2 increased nuclear targeting of NGFI-B. However, results in section 4.4 demonstrated that by mimicking phosphorylation of Thr 142 in NGFI-B, nuclear import of NGFI-B was reduced. It was therefore interesting to investigate whether dominant active or dominant negative ERK2 would increase or decrease nuclear import of NGFI-B-GFP. NGFI-B-GFP was co-transfected with dominant active or dominant negative ERK2 in CV-1 cells, and nuclear FRAP was performed.

The nuclear import of NGFI-B-GFP after photobleaching was reduced by over-expressed dominant active ERK2 (Figure 3.8). This reduction could be a result of the phosphorylation of NGFI-B by ERK2 that was demonstrated by Slagsvold *et al.* (2002). The reduction of nuclear import of NGFI-B by Thr 142 phosphorylation was also suggested by results in section 4.5, in which Thr was mutated to Glu to mimic constitutive phosphorylation of this residue. Furthermore, it was demonstrated that EGF, which activates ERK2, reduced the nuclear import of NGFI-B-GFP.

Visual inspections using the CLSM did not reveal an increased concentration of nuclear NGFI-B-GFP when co-expressed with active ERK2 (data not shown), as previously described by Jacobs and Paulsen (2005). However, in the CV-1 cells used in this thesis, the concentration of NGFI-B-GFP in the nucleus was higher than in the cytoplasm (section 4.4). Consequently, an increased nuclear localization of NGFI-B-GFP would have been difficult to visually detect. However, EGF which activates ERK2 was shown to reduce the nuclear import of NGFI-B-GFP in this thesis, while Jacobs *et al.* demonstrated an increase. This suggests that changes have occurred in the CV-1 cell line or in the serum used in the culture medium (section 4.4). If so, an increase of nuclear concentration of NGFI-B-GFP expressed with dominant active ERK2 in the CV-1 cells used in this thesis might not have taken place. The fact that ERK2 signaling resulted in such different responses in the CV-1 cells could be explained by involvement of ERK2 in regulation of as divergent processes as cell death and proliferation. Although ERK generally has been considered to be involved in a survival signaling pathway, experiments demonstrate that ERK may mediate apoptosis in CGN (Subramaniam *et al.*, 2004), numerous cell lines, and *in vivo* (Zhuang and Schnellmann, 2006).

Nuclear FRAP performed on cells co-expressing NGFI-B-GFP and dominant negative ERK2 demonstrated a reduced nuclear import of NGFI-B-GFP (Figure 3.8). It was previously demonstrated in this thesis that by blocking phosphorylation of Thr 142 by mutation, the nuclear import of NGFI-B was not affected, and that NGFI-B possibly exhibit a basal non-phosphorylation of Thr 142. These results suggest that nuclear import of NGFI-B was not affected by a lack of ERK2 phosphorylation of Thr 142. The reduction of recovery is then likely to have another origin. The over-expression of dominant negative ERK2 could possibly influence a number of cellular processes that affect nuclear import. Preliminary studies (data not shown) also suggest that the reduction of nuclear import of NGFI-B-GFP by dominant negative ERK is non-specific.

4.6 Effects of the MEK/ERK pathway on Glutamate-Induced Cell Death in Cerebellar Granule Neurons

Activation of the MEK/ERK pathway by glutamate via the NMDAR is involved in mammalian memory and learning (Bading and Greenberg, 1991; Kurino *et al.*, 1995; Mao *et al.*, 2004; Perkinton *et al.*, 2002; Platenik *et al.*, 2000). However, activation of ERK during neuropathological over-stimulation of NMDARs may contribute to neuronal death in the adult brain (Jiang *et al.*, 2000). Upon activation, ERK dimerizes and translocates to the nucleus (Khokhlatchev *et al.*, 1998). Such an activation of ERK is induced by EGF, and the effect of EGF stimulation before glutamate exposure was therefore investigated in cultured rat cerebellar granule neurons (CGN). The CGN express glutamate responsive NMDA receptors and are a much used *in vitro* model for studying neuronal apoptosis (Xia *et al.*, 1995a). The glutamate exposure of the CGN represented a relatively mild insult of glutamate toxicity (100 μM) that would initiate apoptosis rather than necrosis. Dying cells were stained with trypan blue and counted.

The results (Figure 3.9) demonstrated a significant reduction of glutamate-induced cell death in CGN that were treated with EGF. The reduction of cell death indicated that EGF had a neuroprotective effect in the CGN, an effect previously presented by Abe and Saito (1992) and Gunn-Moore and Tavare (1998), and that possibly was mediated by the activation of ERK. The relevance of MEK/ERK pathways in neuronal cell survival was documented in PC12 pheochromocytoma cells, in which down-regulation of ERK mediated by NGF withdrawal led to apoptosis, whereas the activation of the ERK signaling pathway by NGF inhibited apoptosis (Xia *et al.*, 1995b). Such a protective effect of ERK could have taken place when cells were treated with EGF, as demonstrated by Jacobs *et al.*, or the protection by EGF could have been mediated through other pathways.

In addition to having a protective effect, the activation of ERK is a consequence of glutamate exposure, in which the phosphorylation of ERK was demonstrated to contribute to neuronal death (Subramaniam *et al.*, 2004; Zhou *et al.*, 2007). In cortical neurons, the cells committed to apoptosis in response to glutamate if the activation of ERK was persistent (Stanciu *et al.*, 2000).

It was therefore interesting to investigate whether MEK inhibitor U0126, which inhibits the MEK/ERK cascade, would inhibit or augment glutamate-induced cell death in CGN if distributed at different time-points. The results (Figure 3.9) demonstrated that MEK-inhibition subsequent to glutamate exposure did not affect glutamate-induced cell death. Consequently, a continuous activation, and thereby sustained nuclear accumulation of ERK, was not involved in the glutamate-mediated cell death of the CGN. However, MEK inhibitor administered prior to glutamate exposure resulted in a small reduction of glutamate-induced cell death (Figure 3.9). This tendency suggests that the MEK/ERK signaling pathway was not involved in survival of the CGN, as this would have resulted in an increased cell death when MEK was inhibited. The small reduction of cell death by early MEK inhibition suggests that ERK somehow was involved in the cell death induced by glutamate. A greater reduction of glutamate-mediated cell death resulting from MEK inhibition in advance of glutamate exposure was previously demonstrated in CGN (Debernard K.B., UIO, personal communication). These results indicate that the early activation, and thereby early nuclear accumulation of activated ERK, is involved in the mediation of glutamate-induced cell death in CGN.

In summary, the subcellular distribution of ERK may be involved in the early promotion of glutamate-induced cell death, and the ERK induced by EGF and glutamate may have different functions in CGN. Multiple functions of ERK could result from two distinct kinds of ERKs that were either activated by EGF via EGF receptors, or by glutamate via the NMDAR. Furthermore, glutamate is previously shown to have different effects on ERK depending on which NMDAR that was activated. Ivanov *et al.* (2006) demonstrated that activation of the NR2B subunit in synaptic NMDAR was responsible for ERK phosphorylation and activation, while stimulation of the extrasynaptic NR2B contributed to ERK dephosphorylation and inactivation.

To further pursue the involvement of ERK in neuronal apoptosis, it would be interesting to examine whether glutamate- and EGF-activated ERK may signal differently to downstream mediators, such as NGFI-B. The CGN appears to be a suitable model for such investigations, due to the glutamate-induced cell death, EGF receptors, activation of ERK by EGF, and possibly by glutamate. To assay whether NGFI-B is equally phosphorylated by glutamate and EGF by using

a proteomic approach would be interesting, as well as to over-express the NGFI-B mutants presented in section 4.4 followed by FRAP studies. In addition, studies of the *wt* protein also have to be conducted, and the effects of glutamate and EGF on the subcellular localization of NGFI-B in the CGN should be investigated.

4.7 The Subcellular Distribution of NGFI-B and AIF in CGN

The subcellular localization of NGFI-B in CGN was investigated in order to establish whether this *in vitro* model was suited for further studies of neuronal traffic of NGFI-B. Mitochondrial association of NGFI-B is demonstrated to result in apoptotic activation of mitochondria, which facilitates the release of apoptotic factors such as AIF (Lin *et al.*, 2004). AIF translocates from the mitochondria to the nucleus, and the subcellular localization AIF was therefore investigated as a marker of apoptotic mitochondrial activation. By double immunostaining of CGN exposed to glutamate or physiological buffer, translocation of NGFI-B to the mitochondria and AIF to the nucleus of the same cell was investigated.

In the majority of CGN that were exposed to glutamate, NGFI-B localized to both the cytoplasm and the nucleus. Such a distribution was similar to that of CGN exposed to physiological buffer, and indicated that there were few apoptotic cells on the glutamate-exposed cover glasses. The immunostained cells were from the same experiments as the cells that were assayed for cell death in section 4.6. Glutamate induced cell death in a majority of such cells, and would also have done so in the immunostained cells. However, the CGN for cell counts were incubated over night subsequent to glutamate exposure, whereas cells for immunostaining were incubated for two hours. Previous studies had shown translocation of AIF in CGN at this time-point (Slagsvold *et al.*, 2003). However, the translocation of NGFI-B was possibly not initiated after two hours in the CGN investigated in this thesis, and additional time-points could reveal if translocation would take place in more cells if they were fixed at a later time. To enable CLSM imaging, the immunostained CGN were grown on glass, whereas CGN for cell counts were grown on plastic. CGN are known to grow poorly on glass, and the cell density on the cover glasses was low compared to cell densities in plastic culture dishes (data not shown). Possibly, the apoptotic cells

displayed an even poorer adherence to glass and fell off or were washed away during the immunostaining procedure.

In a majority of the glutamate-exposed cells, AIF mainly localized to the cytoplasm. The absence of AIF translocation to the nucleus could be an additional indication of few apoptotic cells. In some glutamate-exposed cells, the staining of AIF was strongly reduced and a translocation of AIF would have been difficult to detect.

NGFI-B localized to the cytoplasm, and not the nucleus, in a minority of the glutamate-exposed cells. Such cells appeared to be condensed, and were possibly apoptotic. However, AIF was also localized to the cytoplasm in the condensed cells, and the sole translocation of NGFI-B-GFP possibly indicates that the two processes occur at different times. It was reported by Munoz-Pinedo *et al.* (2006) that the mitochondrial release of AIF proceeds more slowly than the release of other apoptogenic proteins such as cytochrome *c* (hour-range for AIF as compared to minute-range for other apoptogenic proteins), although the release starts simultaneously. Alternatively, the glutamate-induced apoptosis in the CGN was a caspase dependent cell death without caspase-independent pathways involving AIF (discussed with Dawson,T., Johns Hopkins University, USA). In a caspase dependent apoptosis, cytochrome *c* could be used as a marker of mitochondrial activation.

4.8 Conclusions

- A luminometric ATP-assay with over-expressed luciferase from CV-1 cells was established and applied in the validation of ATP depletions.
- The nuclear import of NGFI-B was energy-dependent.
- A Thr to Glu mutation reduced the nuclear import of NGFI-B.
- The nuclear import of NGFI-B was reduced by EGF.
- Co-expression with dominant active ERK2 reduced the nuclear import of NGFI-B.
- Glutamate-induced cell death of CGN was slightly reduced by inhibition of the MEK/ERK pathway.
- CGN may be used as a model for determination of neuronal NGFI-B traffic.

References

Abe, K., and Saito, H. (1992). Protective effect of epidermal growth factor on glutamate neurotoxicity in cultured cerebellar neurons. Neuroscience Research *14*, 117-123.

Alberts, B., Johnson, A., Lewis, J., Raff, M., Roberts, K., and Walter, P. (2002). Molecular Biology Of The Cell, 4 edn (New York: Garland Science).

Allue I, G. O., Dementieva E, Ugarova N, Cobbold P (1996). Evidence for rapid consumption of millimolar concentrations of cytoplasmic ATP during rigor -contracture of metabolically compromised single cardiomyocytes. Biochem J *319*, 463-469.

Armstrong, J. S. (2006). The role of the mitochondrial permeability transition in cell death. Mitochondrion *6*, 225-234.

Asztély, F., and Gustafsson, B. (1996). Ionotropic glutamate receptors. Their possible role in the expression of hippocampal synaptic plasticity. Molecular Neurobiology *12*, 1-11.

Axelrod, D., Koppel, D. E., Schlessinger, J., Elson, E., and Webb, W. W. (1976). Mobility measurement by analysis of fluorescence photobleaching recovery kinetics. Biophysical journal *16*, 1055-1069.

Bading, H., and Greenberg, M. E. (1991). Stimulation of protein tyrosine phosphorylation by NMDA receptor activation. Science *253*, 912-914.

Berg-Johnsen, J., Paulsen, R. E., Fonnum, F., and Langmoen, I. A. (1993). Changes in evoked potentials and amino acid content during fluorocitrate action studied in rat hippocampal cortex. Experimental Brain Research *96*, 241-246.

Bourne, H. R., Sanders, D. A., and McCormick, F. (1990). The GTPase superfamily: a conserved switch for diverse cell functions. Nature *348*, 125-132.

Brewer, L. D., Thibault, O., Staton, J., Thibault, V., Rogers, J. T., Garcia-Ramos, G., Kraner, S., Landfield, P. W., and Porter, N. M. (2007). Increased vulnerability of hippocampal neurons with age in culture: Temporal association with increases in NMDA receptor current, NR2A subunit expression and recruitment of L-type calcium channels. Brain Research *1151*, 20-31.

Cain, K., Bratton, S. B., and Cohen, G. M. (2002). The Apaf-1 apoptosome: a large caspase-activating complex. Biochimie *84*, 203-214.

Casper, D., and Blum, M. (1995). Epidermal Growth Factor and Basic Fibroblast Growth Factor Protect Dopaminergic Neurons from Glutamate Toxicity in Culture. Journal of Neurochemistry *65*, 1016-1026.

Chan, S.-L., and Yu, V. C. (2004). Proteins of the BCL-2 family in apoptosis signalling: from mechanistic insights to therapeutic opportunities. Clinical and Experimental Pharmacology and Physiology *31*, 119-128.

Chang, C., Kokontis, J., Liao, S. S., and Chang, Y. (1989). Isolation and characterization of human TR3 receptor: a member of steroid receptor superfamily. The Journal of steroid biochemistry *34*, 391-395.

Chang, F., Steelman, L. S., Lee, J. T., Shelton, J. G., Navolanic, P. M., Blalock, W. L., Franklin, R. A., and McCubrey, J. A. (2003). Signal transduction mediated by the Ras/Raf/MEK/ERK pathway from cytokine receptors to transcription factors: potential targeting for therapeutic intervention. Leukemia *17*, 1263-1293.

Chen, J., Dai, J., Grant, R. L., Doctor, R. B., Sheetz, M. P., and Mandel, L. J. (1997). Loss of cytoskeletal support is not sufficient for anoxic plasma membrane disruption in renal cells. American journal of physiology Cell physiology *272*, C1319-1328.

Chen, J., Doctor, R. B., and Mandel, L. J. (1994). Cytoskeletal dissociation of ezrin during renal anoxia: role in microvillar injury. American journal of physiology Cell physiology *267*, C784-795.

Chen, J., and Wagner, M. C. (2001). Altered membrane-cytoskeleton linkage and membrane blebbing in energy-depleted renal proximal tubular cells. American journal of physiology Cell physiology *280*, F619-627.

Chen, K. Y., Huang, L. M., Kung, H. J., Ann, D. K., and Shih, H. M. (2004). The role of tyrosine kinase Etk/Bmx in EGF-induced apoptosis of MDA-MB-468 breast cancer cells. Oncogene *23*, 1854-1862.

Chen, P. E., and Wyllie, D. J. A. (2006). Pharmacological insights obtained from structure-function studies of ionotropic glutamate receptors. British journal of pharmacology *147*, 839-853.

Choi, D. W., Koh, J. Y., and Peters, S. (1988). Pharmacology of glutamate neurotoxicity in cortical cell culture: attenuation by NMDA antagonists. The Journal of neuroscience *8*, 185-196.

Ciani, E., and Paulsen, R. E. (1995). Activation of a reporter gene responsive to NGFI-B in cultured neurons and astrocytes. Journal of Molecular Neuroscience *6*, 131-139.

Clark, J., Benjamin, H., Gill, S., Sidhar, S., Goodwin, G., Crew, J., Gusterson, B. A., Shipley, J., and Cooper, C. S. (1996). Fusion of the EWS gene to CHN, a member of the steroid/thyroid receptor gene superfamily, in a human myxoid chondrosarcoma. Oncogene *12*, 229-235.

Contestabile, A. (2002). Cerebellar granule cells as a model to study mechanisms of neuronal apoptosis or survival in vivo and in vitro. The cerebellum *1*, 41-55.

Davis, I. J., Hazel, T. G., Chen, R. H., Blenis, J., and Lau, L. F. (1993). Functional domains and phosphorylation of the orphan receptor Nur77. Molecular endocrinology *7*, 953-964.

de Ortiz, S. P., Cannon, M. M., and Jamieson, G. A. (1994). Expression of nuclear hormone receptors within the rat hippocampus: identification of novel orphan receptors. Molecular Brain Research *23*, 278-283.

Dingledine, R., Borges, K., Bowie, D., and Traynelis, S. F. (1999). The Glutamate Receptor Ion Channels. Pharmacological reviews *51*, 7-62.

Dingwall, C., and Laskey, R. A. (1991). Nuclear targeting sequences--a consensus? Trends in biochemical sciences *16*, 478-481.

Eblen, S. T., Kumar, N. V., Shah, K., Henderson, M. J., Watts, C. K. W., Shokat, K. M., and Weber, M. J. (2003). Identification of Novel ERK2 Substrates through Use of an Engineered Kinase and ATP Analogs. The Journal of biological chemistry *278*, 14926-14935.

Fahrner, T. J., Carroll, S. L., and Milbrandt, J. (1990). The NGFI-B protein, an inducible member of the thyroid/steroid receptor family, is rapidly modified posttranslationally. Molecular and cellular biology *10*, 6454-6459.

Fink, S. L., and Cookson, B. T. (2005). Apoptosis, Pyroptosis, and Necrosis: Mechanistic Description of Dead and Dying Eukaryotic Cells. Infection and immunity *73*, 1907-1916.

Flaig, R., Greschik, H., Peluso-Iltis, C., and Moras, D. (2005). Structural Basis for the Cell-specific Activities of the NGFI-B and the Nurr1 Ligand-binding Domain. The Journal of biological chemistry *280*, 19250-19258.

Fonnum, F. (1984). Glutamate: a neurotransmitter in mammalian brain. Journal of neurochemistry *42*, 1-11.

Frosst, P., Guan, T., Subauste, C., Hahn, K., and Gerace, L. (2002). Tpr is localized within the nuclear basket of the pore complex and has a role in nuclear protein export. The Journal of cell biology *156*, 617-630.

Gallo, V., Kingsbury, A., Balazs, R., and Jorgensen, O. S. (1987). The role of depolarization in the survival and differentiation of cerebellar granule cells in culture. The journal of neuroscience *7*, 2203-2213.

Gardoni, F., and Di Luca, M. (2006). New targets for pharmacological intervention in the glutamatergic synapse. European Journal of Pharmacology *545*, 2-10.

Gerber, A. M., and Vallano, M. L. (2006). Structural properties of the NMDA receptor and the design of neuroprotective therapies. Mini reviews in medicinal chemistry *6*, 805-815.

Goda, K., Nagy, H., Mechetner, E., Cianfriglia, M., and Szabo, G., Jr. (2002). Effects of ATP depletion and phosphate analogues on P-glycoprotein conformation in live cells. European journal of biochemistry *269*, 2672-2677.

Gogvadze, V., and Orrenius, S. (2006). Mitochondrial regulation of apoptotic cell death. Chemico-Biological Interactions *163*, 4-14.

Gorlich, D., Kostka, S., Kraft, R., Dingwall, C., Laskey, R. A., Hartmann, E., and Prehn, S. (1995). Two different subunits of importin cooperate to recognize nuclear localization signals and bind them to the nuclear envelope. Current Biology *5*, 383-392.

Graham, F. L., and van der Eb, A. J. (1973). A new technique for the assay of infectivity of human adenovirus 5 DNA. Virology *52*, 456-467.

Gunn-Moore, F. J., and Tavare, J. M. (1998). Apoptosis of cerebellar granule cells induced by serum withdrawal, glutamate or [beta]-amyloid, is independent of Jun kinase or p38 mitogen activated protein kinase activation. Neuroscience Letters *250*, 53-56.

Haggie, P. M., Stanton, B. A., and Verkman, A. S. (2002). Diffusional Mobility of the Cystic Fibrosis Transmembrane Conductance Regulator Mutant, Delta F508-CFTR, in the Endoplasmic Reticulum Measured by Photobleaching of GFP-CFTR Chimeras. The Journal of biological chemistry *277*, 16419-16425.

Han, Y. H., Cao, X., Lin, B., Lin, F., Kolluri, S. K., Stebbins, J., Reed, J. C., Dawson, M. I., and Zhang, X. k. (2006). Regulation of Nur77 nuclear export by c-Jun N-terminal kinase and Akt. Oncogene *25*, 2974-2986.

Hazel, T. G., Misra, R., Davis, I. J., Greenberg, M. E., and Lau, L. F. (1991). Nur77 is differentially modified in PC12 cells upon membrane depolarization and growth factor treatment. Molecular and cellular biology *11*, 3239-3246.

Hazel, T. G., Nathans, D., and Lau, L. F. (1988). A Gene Inducible by Serum Growth Factors Encodes a Member of the Steroid and Thyroid Hormone Receptor Superfamily. Proceedings of the National Academy of Sciences of the United States of America *85*, 8444-8448.

Hedvat, C. V., and Irving, S. G. (1995). The isolation and characterization of MINOR, a novel mitogen-inducible nuclear orphan receptor. Journal of molecular endocrinology *9*, 1692-1700.

Hirata, Y., Kiuchi, K., Chen, H. C., Milbrandt, J., and Guroff, G. (1993). The phosphorylation and DNA binding of the DNA-binding domain of the orphan nuclear receptor NGFI-B. The Journal of biological chemistry *268*, 24808-24812.

Hopps, H. E., Bernheim, B. C., Nisalak, A., Tjio, J. H., and Smadel, J. E. (1963). Biologic Characteristics of a Continuous Kidney Cell Line Derived from the African Green Monkey. The journal of immunology *91*, 416-424.

Hsu, H. C., Zhou, T., and Mountz, J. D. (2004). Nur77 family of nuclear hormone receptors. Current drug targets Inflammation & allergy *3*, 413-423.

Ivanov, A., Pellegrino, C., Rama, S., Dumalska, I., Salyha, Y., Ben-Ari, Y., and Medina, I. (2006). Opposing role of synaptic and extrasynaptic NMDA receptors in regulation of the

extracellular signal-regulated kinases (ERK) activity in cultured rat hippocampal neurons. The Journal of physiology *572*, 789-798.

Jacobs, C. M., Boldingh, K. A., Slagsvold, H. H., Thoresen, G. H., and Paulsen, R. E. (2004). ERK2 Prohibits Apoptosis-induced Subcellular Translocation of Orphan Nuclear Receptor NGFI-B/TR3. The Journal of biological chemistry *279*, 50097-50101.

Jiang, Q., Gu, Z., Zhang, G., and Jing, G. (2000). Diphosphorylation and involvement of extracellular signal-regulated kinases (ERK1/2) in glutamate-induced apoptotic-like death in cultured rat cortical neurons. Brain Research *857*, 71-77.

Jiang, X., and Wang, X. (2000). Cytochrome c Promotes Caspase-9 Activation by Inducing Nucleotide Binding to Apaf-1. The Journal of biological chemistry *275*, 31199-31203.

Johnson, J. W., and Ascher, P. (1987). Glycine potentiates the NMDA response in cultured mouse brain neurons. Nature *325*, 529-531.

Jorissen, R. N., Walker, F., Pouliot, N., Garrett, T. P. J., Ward, C. W., and Burgess, A. W. (2003). Epidermal growth factor receptor: mechanisms of activation and signalling. Experimental Cell Research *284*, 31-53.

Kagaya, S. S., Ohkura, N. N., Tsukada, T. T., Miyagawa, M. M., Sugita, Y. Y., Tsujimoto, G. G., Matsumoto, K. K., Saito, H. H., and Hashida, R. R. (2005). Prostaglandin A2 acts as a transactivator for NOR1 (NR4A3) within the nuclear receptor superfamily. Biological & pharmaceutical bulletin *28*, 1603-1607.

Kang, H. J., Song, M. J., Choung, S. Y., Kim, S. J., and Le, M. O. (2000). Transcriptional induction of Nur77 by indomethacin that results in apoptosis of colon cancer cells. Biological & pharmaceutical bulletin *23*, 815-819.

Kerr, J. F., Wyllie, A. H., and Currie, A. R. (1972). Apoptosis: a basic biological phenomenon with wide-ranging implications in tissue kinetics. The British journal of cancer *26*, 239-257.

Khokhlatchev, A. V., Canagarajah, B., Wilsbacher, J., Robinson, M., Atkinson, M., Goldsmith, E., and Cobb, M. H. (1998). Phosphorylation of the MAP Kinase ERK2 Promotes Its Homodimerization and Nuclear Translocation. Cell *93*, 605-615.

Klein, J. A., Longo-Guess, C. M., Rossmann, M. P., Seburn, K. L., Hurd, R. E., Frankel, W. N., Bronson, R. T., and Ackerman, S. L. (2002). The harlequin mouse mutation downregulates apoptosis-inducing factor. Nature *419*, 367-374.

Kolluri, S. K., Bruey-Sedano, N., Cao, X., Lin, B., Lin, F., Han, Y.-H., Dawson, M. I., and Zhang, X.-k. (2003). Mitogenic Effect of Orphan Receptor TR3 and Its Regulation by MEKK1 in Lung Cancer Cells. Molecular and cellular biology *23*, 8651-8667.

Kottke, T. J., Blajeski, A. L., Martins, L. M., Mesner, P. W., Jr., Davidson, N. E., Earnshaw, W. C., Armstrong, D. K., and Kaufmann, S. H. (1999). Comparison of Paclitaxel-, 5-Fluoro-2'-

deoxyuridine-, and Epidermal Growth Factor (EGF)-induced Apoptosis. EVIDENCE FOR EGF-INDUCED ANOIKIS. The Journal of biological chemistry *274*, 15927-15936.

Kristiansen, L. V., Huerta, I., Beneyto, M., and Meador-Woodruff, J. H. (2007). NMDA receptors and schizophrenia. Current Opinion in Pharmacology *7*, 48-55.

Kurino, M., Fukunaga, K., Ushio, Y., and Miyamoto, E. (1995). Activation of mitogen-activated protein kinase in cultured rat hippocampal neurons by stimulation of glutamate receptors. Journal of neurochemistry *65*, 1282-1289.

Kuryatov, A., Laube, B., Betz, H., and Kuhse, J. (1994). Mutational analysis of the glycine-binding site of the NMDA receptor: Structural similarity with bacterial amino acid-binding proteins. Neuron *12*, 1291-1300.

Labelle, Y., Zucman, J., Stenman, G., Kindblom, L.-G., Knight, J., Turc-Carel, C., Dockhorn-Dworniczak, B., Mandahl, N., Desmaze, C., Peter, M.*, et al.* (1995). Oncogenic conversion of a novel orphan nuclear receptor by chromosome translocation. Human molecular genetics *4*, 2219-2226.

Lange, A., Mills, R. E., Lange, C. J., Stewart, M., Devine, S. E., and Corbett, A. H. (2007). Classical Nuclear Localization Signals: Definition, Function, and Interaction with Importin {alpha}. The Journal of biological chemistry *282*, 5101-5105.

Laube, B., Hirai, H., Sturgess, M., Betz, H., and Kuhse, J. (1997). Molecular Determinants of Agonist Discrimination by NMDA Receptor Subunits: Analysis of the Glutamate Binding Site on the NR2B Subunit. Neuron *18*, 493-503.

Law, S. W., Conneely, O. M., DeMayo, F. J., and O'Malley, B. W. (1992). Identification of a new brain-specific transcription factor, NURR1. Journal of molecular endocrinology *6*, 2129-2135.

Li, H., Kolluri, S. K., Gu, J., Dawson, M. I., Cao, X., Hobbs, P. D., Lin, B., Chen, G.-q., Lu, J.-s., Lin, F.*, et al.* (2000). Cytochrome c Release and Apoptosis Induced by Mitochondrial Targeting of Nuclear Orphan Receptor TR3. Science *289*, 1159-1164.

Li, Y., Lin, B., Agadir, A., Liu, R. R., Dawson, M. I., Reed, J. C., Fontana, J. A., Bost, F., Hobbs, P. D., Zheng, Y.*, et al.* (1998). Molecular determinants of AHPN (CD437)-induced growth arrest and apoptosis in human lung cancer cell lines. Molecular and cellular biology *18*, 4719-4731.

Lin, B., Kolluri, S. K., Lin, F., Liu, W., Han, Y.-H., Cao, X., Dawson, M. I., Reed, J. C., and Zhang, X.-k. (2004). Conversion of Bcl-2 from Protector to Killer by Interaction with Nuclear Orphan Receptor Nur77/TR3. Cell *116*, 527-540.

Lucas, D. R., and Newhouse, J. P. (1957). The toxic effect of sodium L-glutamate on the inner layers of the retina. AMA archives of ophthalmology *58*, 193-201.

Mangelsdorf, D. J., and Evans, R. M. (1995). The RXR heterodimers and orphan receptors. Cell *83*, 841-850.

Mao, L., Tang, Q., Samdani, S., Liu, Z., and Wang, J. Q. (2004). Regulation of MAPK/ERK phosphorylation via ionotropic glutamate receptors in cultured rat striatal neurons. The European journal of neuroscience *19*, 1207-1216.

Maren, S., and Baudry, M. (1995). Properties and Mechanisms of Long-Term Synaptic Plasticity in the Mammalian Brain: Relationships to Learning and Memory. Neurobiology of Learning and Memory *63*, 1-18.

Martinez-Gonzalez, J., and Badimon, L. (2005). The NR4A subfamily of nuclear receptors: new early genes regulated by growth factors in vascular cells. Cardiovascular Research *65*, 609-618.

Masuyama, N., Oishi, K., Mori, Y., Ueno, T., Takahama, Y., and Gotoh, Y. (2001). Akt Inhibits the Orphan Nuclear Receptor Nur77 and T-cell Apoptosis. J Biol Chem *276*, 32799-32805.

Meinke, G., and Sigler, P. B. (1999). DNA-binding mechanism of the monomeric orphan nuclear receptor NGFI-B. Nature structural & molecular biology *6*, 471-477.

Milbrandt, J. (1988). Nerve growth factor induces a gene homologous to the glucocorticoid receptor gene. Neuron *1*, 183-188.

Moen, L. F. (2007) RARα regulates the interaction between RXRα and NGFI-B in response to specific ligands, Master Thesis, University of Oslo, Oslo.

Moll, U. M., Marchenko, N., and Zhang, X. k. (2006). p53 and Nur77//TR3 - transcription factors that directly target mitochondria for cell death induction. Oncogene *25*, 4725-4743.

Mori, H., Masaki, H., Yamakura, T., and Mishina, M. (1992). Identification by mutagenesis of a Mg2+ -block site of the NMDA receptor channel. Nature *358*, 673-675.

Mourad, N., and Parks, R. E. (1965). NDP Kinase: Demonstration of Phosphorylated Enzyme as the Reactive Intermediate. Biochemical and biophysical research communications *19*, 312-316.

Munoz-Pinedo, C., Guio-Carrion, A., Goldstein, J. C., Fitzgerald, P., Newmeyer, D. D., and Green, D. R. (2006). Different mitochondrial intermembrane space proteins are released during apoptosis in a manner that is coordinately initiated but can vary in duration. Proceedings of the National Academy of Sciences of the United States of America *103*, 11573-11578.

Nishi, M., Hinds, H., Lu, H.-P., Kawata, M., and Hayashi, Y. (2001). Motoneuron-Specific Expression of NR3B, a Novel NMDA-Type Glutamate Receptor Subunit That Works in a Dominant-Negative Manner. The journal of neuroscience *21*, 185RC-.

Ohkura, N., Hijikuro, M., Yamamoto, A., and Miki, K. (1994). Molecular Cloning of a Novel Thyroid/Steroid Receptor Superfamily Gene from Cultured Rat Neuronal Cells. Biochemical and Biophysical Research Communications *205*, 1959-1965.

Okabe, T., Takayanagi, R., Imasaki, K., Haji, M., Nawata, H., and Watanabe, T. (1995). cDNA cloning of a NGFI-B/nur77-related transcription factor from an apoptotic human T cell line. The journal of immunology *154*, 3871-3879.

Olney, J. W. (1969). Glutaate-induced retinal degeneration in neonatal mice. Electron microscopy of the acutely evolving lesion. Journal of neuropathology and experimental neurology *28*, 455-474.

Paoletti, P., and Neyton, J. (2007). NMDA receptor subunits: function and pharmacology. Current Opinion in Pharmacology *7*, 39-47.

Pekarsky, Y., Hallas, C., Palamarchuk, A., Koval, A., Bullrich, F., Hirata, Y., Bichi, R., Letofsky, J., and Croce, C. M. (2001). Akt phosphorylates and regulates the orphan nuclear receptor Nur77. Proceedings of the National Academy of Sciences of the United States of America *98*, 3690-3694.

Perkinton, M. S., Ip, J., Wood, G. L., Crossthwaite, A. J., and Williams, R. J. (2002). Phosphatidylinositol 3-kinase is a central mediator of NMDA receptor signalling to MAP kinase (Erk1/2), Akt/PKB and CREB in striatal neurones. Journal of Neurochemistry *80*, 239-254.

Philips, A., Lesage, S., Gingras, R., Maira, M. M., Gauthier, Y., Hugo, P., and Drouin, J. (1997). Novel dimeric Nur77 signaling mechanism in endocrine and lymphoid cells. Molecular and cellular biology *17*, 5946-5951.

Platenik, J., Kuramoto, N., and Yoneda, Y. (2000). Molecular mechanisms associated with long-term consolidation of the NMDA signals. Life Sciences *67*, 335-364.

Poon, I. K. H., and Jans, D. A. (2005). Regulation of Nuclear Transport: Central Role in Development and Transformation? Traffic *6*, 173-186.

Proskuryakov, S. Y. a., Konoplyannikov, A. G., and Gabai, V. L. (2003). Necrosis: a specific form of programmed cell death? Experimental Cell Research *283*, 1-16.

Quimby, B. B., and Dasso, M. (2003). The small GTPase Ran: interpreting the signs. Current Opinion in Cell Biology *15*, 338-344.

Robbins, J., Dilwortht, S. M., Laskey, R. A., and Dingwall, C. (1991). Two interdependent basic domains in nucleoplasmin nuclear targeting sequence: Identification of a class of bipartite nuclear targeting sequence. Cell *64*, 615-623.

Sasaki, Y. F., Rothe, T., Premkumar, L. S., Das, S., Cui, J., Talantova, M. V., Wong, H.-K., Gong, X., Chan, S. F., Zhang, D.*, et al.* (2002). Characterization and Comparison of the NR3A Subunit of the NMDA Receptor in Recombinant Systems and Primary Cortical Neurons. Journal of neurophysiology *87*, 2052-2063.

Scearce, L. M., Laz, T. M., Hazel, T. G., Lau, L. F., and Taub, R. (1993). RNR-1, a nuclear receptor in the NGFI-B/Nur77 family that is rapidly induced in regenerating liver. The Journal of biological chemistry *268*, 8855-8861.

Schwoebel, E. D., Ho, T. H., and Moore, M. S. (2002). The mechanism of inhibition of Ran-dependent nuclear transport by cellular ATP depletion. The Journal of cell biology *157*, 963-974.

Seliger, H. H., McElroy, W. D., White, E. H., and Field, G. F. (1961). Stereo-specificity and firefly bioluminescence, a comparison of natural and synthetic luciferins. Proceedings of the National Academy of Sciences of the United States of America *47*, 1129-1134.

Slagsvold, H. H., Ostvold, A.-C., Fallgren, A. B., and Paulsen, R. E. (2002). Nuclear Receptor and Apoptosis Initiator NGFI-B Is a Substrate for Kinase ERK2. Biochemical and Biophysical Research Communications *291*, 1146-1150.

Slagsvold, H. H., Rosseland, C. M., Jacobs, C., Khuong, E., Kristoffersen, N., Gaarder, M., Fallgren, A. B., Huitfeldt, H. S., and Paulsen, R. E. (2003). High molecular weight DNA fragments are processed by caspase sensitive or caspase independent pathways in cultures of cerebellar granule neurons. Brain Research *984*, 111-121.

Smith, A. E., Slepchenko, B. M., Schaff, J. C., Loew, L. M., and Macara, I. G. (2002). Systems Analysis of Ran Transport. Science *295*, 488-491.

Stanciu, M., Wang, Y., Kentor, R., Burke, N., Watkins, S., Kress, G., Reynolds, I., Klann, E., Angiolieri, M. R., Johnson, J. W., and DeFranco, D. B. (2000). Persistent Activation of ERK Contributes to Glutamate-induced Oxidative Toxicity in a Neuronal Cell Line and Primary Cortical Neuron Cultures. The Journal of biological chemistry *275*, 12200-12206.

Stewart, M. (2007). Molecular mechanism of the nuclear protein import cycle. Nature reviews Molecular cell biology *8*, 195-208.

Subramaniam, S., Zirrgiebel, U., von Bohlen und Halbach, O., Strelau, J., Laliberte, C., Kaplan, D. R., and Unsicker, K. (2004). ERK activation promotes neuronal degeneration predominantly through plasma membrane damage and independently of caspase-3. The Journal of cell biology *165*, 357-369.

Sucher, N., Akbarian, S., Chi, C., Leclerc, C., Awobuluyi, M., Deitcher, D., Wu, M., Yuan, J., Jones, E., and Lipton, S. (1995). Developmental and regional expression pattern of a novel NMDA receptor-like subunit (NMDAR-L) in the rodent brain. The journal of neuroscience *15*, 6509-6520.

Susin, S. A., Lorenzo, H. K., Zamzami, N., Marzo, I., Snow, B. E., Brothers, G. M., Mangion, J., Jacotot, E., Costantini, P., Loeffler, M.*, et al.* (1999). Molecular characterization of mitochondrial apoptosis-inducing factor. Nature *397*, 441-446.

Vahsen, N., Candé, C., Brière, J. J., Bénit, P., Joza, N., Larochette, N., Mastroberardino, P. G., Pequignot, M. O., Casares, N., Lazar, V., *et al.* (2004). AIF deficiency compromises oxidative phosphorylation. The EMBO journal *23*, 4679-4689.

Vaudry, D., Falluel-Morel, A., Leuillet, S., Vaudry, H., and Gonzalez, B. J. (2003). Regulators of Cerebellar Granule Cell Development Act Through Specific Signaling Pathways. Science *300*, 1532-1534.

Wang, Z., Benoit, G., Liu, J., Prasad, S., Aarnisalo, P., Liu, X., Xu, H., Walker, N. P. C., and Perlmann, T. (2003). Structure and function of Nurr1 identifies a class of ligand-independent nuclear receptors. Nature *423*, 555-560.

Wansa, K. D. S. A., Harris, J. M., Yan, G., Ordentlich, P., and Muscat, G. E. O. (2003). The AF-1 Domain of the Orphan Nuclear Receptor NOR-1 Mediates Trans-activation, Coactivator Recruitment, and Activation by the Purine Anti-metabolite 6-Mercaptopurine. The Journal of biological chemistry *278*, 24776-24790.

Watson, M. A., and Milbrandt, J. (1990). Expression of the nerve growth factor-regulated NGFI-A and NGFI-B genes in the developing rat. Development *110*, 173-183.

Wheeler, M., Stachlewitz, R. F., Yamashina, S., Ikejima, K., Morrow, A. L., and Thurman, R. G. (2000). Glycine-gated chloride channels in neutrophils attenuate calcium influx and superoxide production. The FASEB journal : official publication of the Federation of American Societies for Experimental Biology *14*, 476-484.

Wilson, T., Fahrner, T., Johnston, M., and Milbrandt, J. (1991). Identification of the DNA binding site for NGFI-B by genetic selection in yeast. Science *252*, 1296-1300.

Wilson, T. T. E., Paulsen, R. R. E., Padgett, K. K. A., and Milbrandt, J. J. (1992). Participation of non-zinc finger residues in DNA binding by two nuclear orphan receptors. Science *256*, 107-110.

Wingate, A., and Arthur, J. (2006). Post-translational control of Nur77. Biochemical society transactions *34*, 1107-1109.

Wingate, A. D., Campbell, D. G., Peggie, M., and Arthur, J. S. (2006). Nur77 is phosphorylated in cells by RSK in response to mitogenic stimulation. The Biochemical journal *393*, 715-724.

Woronicz, J. D., Lina, A., Calnan, B. J., Szychowski, S., Cheng, L., and Winoto, A. (1995). Regulation of the Nur77 orphan steroid receptor in activation-induced apoptosis. Molecular and cellular biology *15*, 6364-6376.

Xia, Y., Ragan, R., Seah, E., Michaelis, M., and Michaelis, E. (1995a). Developmental expression of N-methyl-D-aspartate (NMDA)-induced neurotoxicity, NMDA receptor function, and the NMDAR1 and glutamate-binding protein subunits in cerebellar granule cells in primary cultures. Neurochemical Research *20*, 617-629.

Xia, Z., Dickens, M., Raingeaud, J., Davis, R., and Greenberg, M. (1995b). Opposing effects of ERK and JNK-p38 MAP kinases on apoptosis. Science *270*, 1326-1331.

Xiao, Z., Liu, X., Henis, Y. I., and Lodish, H. F. (2000). A distinct nuclear localization signal in the N terminus of Smad 3 determines its ligand-induced nuclear translocation. Proceedings of the National Academy of Sciences of the United States of America *97*, 7853-7858.

Yang, N.-C., Ho, W.-M., Chen, Y.-H., and Hu, M.-L. (2002). A Convenient One-Step Extraction of Cellular ATP Using Boiling Water for the Luciferin-Luciferase Assay of ATP. Analytical Biochemistry *306*, 323-327.

Zeiss, C. J. (2003). The Apoptosis-Necrosis Continuum: Insights from Genetically Altered Mice. Veterinary pathology *40*, 481-495.

Zetterstroum, L., H., R., Solomin, L., Jansson, L., Hoffer, B. J., Olson, L., and Perlmann, T. (1997). Dopamine Neuron Agenesis in Nurr1-Deficient Mice. Science *276*, 248-250.

Zhang, X. K. (2007). Targeting Nur77 translocation. Expert Opinion on Therapeutic Targets *11*, 69-79.

Zhao, X., Dai, W., Zhu, H., Zhang, Y., Cao, L., Ye, Q., Lei, P., and Shen, G. (2006). Epidermal growth factor (EGF) induces apoptosis in a transfected cell line expressing EGF receptor on its membrane. Cell Biology International *30*, 653-658.

Zhou, R. H., Yan, H., Wang, B. R., Kuang, F., Duan, X. L., and Xu, Z. (2007). Role of extracellular signal-regulated kinase in glutamate-stimulated apoptosis of rat retinal ganglion cells. Current eye research *32*, 233-239.

Zhuang, S., and Schnellmann, R. G. (2006). A Death-Promoting Role for Extracellular Signal-Regulated Kinase. The Journal of pharmacology and experimental therapeutics *319*, 991-997.

Appendix

Appendix 1: Chemicals and biological products

Product	***Manufacturer***
AIF (D-20) Mouse anti-goat polyclonal IgG (Lot C2906)	Santa Cruz Biotechnology, Inc. California,USA.
Ara-C	Sigma-Aldrich Co. St. Louis, USA.
ATP	Sigma-Aldrich Co.
BES	Sigma-Aldrich Co.
BME	Invitrogen Co. California, USA.
BSA	Invitrogen Co.
$CaCl_2$	Merck & Co., Inc. New Jersey, USA.
Cy™ 3-conjugated mouse anti-rabbit IgG	Jackson ImmunoResearch Laboratories, Inc. Pennsylvania, USA.
DAPI	Sigma-Aldrich Co.
D-Luciferin	Duchefa Haarlem, The Netherlands.
D-MEM	Invitrogen Co.
DMSO	Sigma-Aldrich Co.
DnaseI	Sigma-Aldrich Co.
DTT	Sigma-Aldrich Co.
EGF	PeproTech Inc. New Jersey, USA.
FBS	Invitrogen Co.
FITC Mouse anti-goat IgG (No AP1867)	Millipore Co. Massachusetts, USA.
FluoroSave™ Reagent	EMD Chamicals California, USA.
Gentamicin sulfate	Sigma-Aldrich Co.
Glucose	Merck & Co., Inc.
Glycine	Sigma-Aldrich Co.
HEPES	Sigma-Aldrich Co.

KCl	Genzyme Pharmaceuticals Massachusetts, USA.
KH_2PO_4	Merck & Co., Inc.
L-Glutamate	Sigma-Aldrich Co.
L-Glutamine	Sigma-Aldrich Co.
MEK inhibitor U0126	Promega Co. Wisconsin, USA.
MES	Sigma-Aldrich Co.
$Mg(CH_3COO)_2$	Merck & Co., Inc.
$MgCl_2$ x $7H_2O$	Merck & Co., Inc.
$MgSO_4$	Merck & Co., Inc.
Na pyruvate	Sigma-Aldrich Co.
$Na_2HPO_4 \cdot H_2$	Merck & Co., Inc.
NaCl	Mallinckrodt Baker B.V. Deventer, The Netherlands.
$NaHCO_3$	Sigma-Aldrich Co.
NaN_3	Merck & Co., Inc.
Normal mouse serum	Jackson ImmunoResearch Laboratories, Inc.
Nur-77 (M-210) Mouse anti-rabbit polyclonal IgG (Lot E1106)	Santa Cruz Biotechnology, Inc.
Penicillin-streptomycin (10 000U/ml / 10 000µl/ml)	Invitrogen Co.
PFA	Electron Microscopy Sciences Pennsylvania, USA.
Phenol red	Merck & Co., Inc.
Poly-L-lysine	Sigma-Aldrich Co.
TCA	Sigma-Aldrich Co.
Tris	MP Biomedicals Ohio, USA
Triton X-100	Sigma-Aldrich Co.
Trypan blue	Sigma-Aldrich Co.
Trypsin	Sigma-Aldrich Co.
Trypsin inhibitor	Sigma-Aldrich Co.
Trypsin-EDTA	Invitrogen Co.